Why the Forcing from Carbon Dioxide Scales as the Logarithm of Its Concentration

DAVID M. ROMPS,[a,b] JACOB T. SEELEY,[c] AND JACOB P. EDMAN[d]

[a] *Department of Earth and Planetary Science, University of California, Berkeley, California*
[b] *Climate and Ecosystem Sciences Division, Lawrence Berkeley National Laboratory, Berkeley, California*
[c] *Department of Earth and Planetary Sciences, Harvard University, Cambridge, Massachusetts*
[d] *KoBold Metals, Berkeley, California*

ABSTRACT: The radiative forcing from carbon dioxide is approximately logarithmic in its concentration, producing about 4 W m^{-2} of global-mean forcing for each doubling. Although these are basic facts of climate science, competing explanations for them have been given in the literature. Here, the reasons for the logarithmic forcing of carbon dioxide are explored in detail and a simplified model for the forcing is constructed. An essential component is the particular distribution of absorption coefficients within the 15-μm band of carbon dioxide. An alternative explanation, which does not depend on the spectrum of carbon dioxide but instead hinges on the tropospheric lapse rate, is shown to be neither necessary nor sufficient to explain the logarithmic forcing of carbon dioxide and to be generally inapplicable to well-mixed greenhouse gases in Earth's atmosphere.

KEYWORDS: Carbon dioxide; Radiative forcing; Radiative transfer

1. Introduction

It is well known that the radiative forcing from carbon dioxide is approximately logarithmic in its concentration, producing about 4 W m^{-2} of additional global-mean forcing for every doubling. There are, however, two different explanations in the literature for this logarithmic dependence. Given the dominant role that CO_2 plays in global warming, this mechanistic uncertainty merits resolution.

Perhaps the most widely accepted explanation is that the logarithmic behavior stems from the particular absorption spectrum of CO_2 (Pierrehumbert 2010, 2011; Wilson and Gea-Banacloche 2012; Jeevanjee et al. 2021). Many absorption bands of greenhouse gases can be approximated with an absorption coefficient κ (m^2 mol^{-1}) that decays exponentially from the band center as a function of frequency or wavenumber (Edwards and Menard 1964a,b) and the 15-μm band[1] of carbon dioxide is a particularly good example of this (Crisp et al. 1986). Heuristic arguments have been given as to why this would lead to a logarithmic forcing (Pierrehumbert 2010, 2011) and analytic calculations have even succeeded in reproducing the $\approx$4 W m^{-2} of forcing from a doubling of CO_2

(Wilson and Gea-Banacloche 2012; Jeevanjee et al. 2021). Notably, this explanation does not depend on the value or even existence of a tropospheric lapse rate.

The competing explanation is what we might call the "lapse-rate theory," which posits that the forcing stems from the troposphere's lapse rate (Sloan and Wolfendale 2013; Huang and Bani Shahabadi 2014; North and Kim 2017). In brief, the lapse-rate theory states that the emission-to-space heights of individual wavenumbers move upward in the troposphere (to lower temperature) a distance that is proportional to the logarithm of the gas concentration, thereby generating a forcing that scales as the log of the concentration. Critically, this theory predicts that the forcing is proportional to the tropospheric lapse rate. Notably, this explanation does not require the absorption coefficients to be distributed logarithmically or in any other special way. We will see that the lapse-rate theory is neither necessary nor sufficient to explain the logarithmic forcing of carbon dioxide (see section 9) and that it generally cannot hold for a well-mixed greenhouse gas in Earth's atmosphere (see section 10).

The aim of this paper is to set the explanation of Pierrehumbert (2010, see his Fig. 4.12) on a firm foundation by demonstrating the properties that lead to carbon dioxide's logarithmic forcing, building a simplified analytic model to showcase the underlying processes, and showing that a line-by-line radiative transfer model gives a logarithmic forcing for the same reasons. This will occupy the bulk of paper, from sections 5 to 8. The reader who wants to quickly learn the basic mechanism may be satisfied with the overview in section 3 and could skip ahead to that section now.

2. Preliminaries

To reduce the problem to its essential elements, we will focus on the instantaneous top-of-atmosphere (TOA) forcing in dry atmospheres. These simplifications (TOA and dry) are

---

[1] To be precise, the 15-μm band is actually a collection of vibrational bands and so is sometimes called a "band of bands" or a "band system." The strongest bands within the 15-μm band are generated by transitions between the vibrational ground state and the first mode of bending, between the first mode of bending and the first mode of symmetric stretching, and between the first and second modes of bending (Kiehl and Ramanathan 1983).

The first two authors contributed equally to this work.

Corresponding author: David M. Romps, romps@berkeley.edu

acceptable because the logarithmic scaling of the CO_2 forcing does not depend on these choices. Figure 1 illustrates this point using radiative-transfer calculations in a three-dimensional snapshot from a cloud-resolving simulation of a tropical atmosphere.[2] Figure 1a shows, plotted as circles, the total, instantaneous, tropopause, longwave forcing from carbon dioxide (averaged over the domain of this snapshot) as a function of the carbon dioxide concentration; the best-fit line is overlaid to emphasize the linearity.

Here and throughout, we will use the variable F to denote an instantaneous longwave forcing, which has dimensions of power per area and whose typically positive values indicate a net downwelling flux of radiative energy. With the exception of Fig. 1a, all forcings discussed in this paper will be calculated at the top of the atmosphere. We will dress F with various subscripts and superscripts to clarify what type of forcing is being used. For example, $F^{tot}(q)$ will be the total forcing from the presence of a well-mixed greenhouse gas at a volume fraction of q. In particular, $F^{tot}(q)$ is the TOA upwelling longwave flux with the greenhouse gas removed minus the TOA upwelling longwave flux with the greenhouse gas's volume fraction set to q. In later sections, we will also discuss $F^{2\times}(q) \equiv F^{tot}(2q) - F^{tot}(q)$, which is the forcing from a doubling of the gas concentration.

From the linearity of the data on the logarithmic axis of Fig. 1a, we see that the all-sky forcing from CO_2 at the tropopause is logarithmic in its concentration to good approximation over a wide range of concentrations (i.e., the 10 doublings shown here). The instantaneous *tropopause* forcing is considered a better proxy for the stratosphere-adjusted forcing than the instantaneous *top-of-atmosphere* forcing (Hansen et al. 1997), but the logarithmic scaling is preserved in the TOA forcing as shown in Fig. 1b. Of the two forcings, the TOA forcing is easier to conceptualize because it only involves upwelling fluxes; therefore, the focus of this paper will be on the TOA forcing. In Fig. 1c, the clouds in the snapshot have been made transparent to infrared radiation, but this does not alter the logarithmic dependence. In Fig. 1d, the water vapor in the snapshot is also made transparent to radiation; again the logarithmic dependence remains. We see, therefore, that the logarithmic dependence of the CO_2 forcing is a phenomenon that does not depend on the presence of water vapor or clouds, or on whether the forcing is measured

at the tropopause or TOA. Therefore, in the sections that follow, all forcings will be calculated at the top of the atmosphere and we will work exclusively with dry atmospheres. For an extension to moist atmospheres, see Jeevanjee et al. (2021).

To probe the mechanism of the logarithmic dependence, we will use a line-by-line radiative transfer model. Although the logarithmic dependence is robust across radiative transfer models, a line-by-line model provides spectral fluxes that are straightforward to interpret. The line-by-line model used here is the Reference Forward Model (RFM; Dudhia 2017), which we use with the HITRAN2016 spectroscopic database (Gordon et al. 2017) and flags MIX, CHI, and CTM to implement the line-mixing model of Strow et al. (1994), to apply the line-shape correction χ factor (Le Doucen et al. 1985; Cousin et al. 1985), and to include the CO_2 continuum. Here, and throughout the paper, air is defined to be 21% oxygen by volume with the remaining fraction apportioned among nitrogen and carbon dioxide. Nitrogen and oxygen are treated as transparent to infrared radiation. Since shortwave absorption by CO_2 alters its forcing by only about 4% (Myhre et al. 1998; Etminan et al. 2016), shortwave fluxes are ignored here for simplicity. Unless otherwise specified, the RFM is used with a vertical spacing of $\Delta\log_{10}(p) = 0.05$ and wavenumbers are sampled at a spacing of 0.01 cm^{-1}.

We focus here on the 15-μm band of CO_2 because it is the source of the vast majority of the forcing from CO_2 at modern atmospheric concentrations (Augustsson and Ramanathan 1977; Zhong and Haigh 2013; Mlynczak et al. 2016), as can be seen by comparing the top and middle panels of Fig. 2. One of the reasons the 15-μm band dominates the forcing is because the Planck distribution peaks near 15 μm at terrestrial temperatures. The bottom panel of Fig. 2 shows the Planck distribution for two different temperatures. The Planck distribution B (W m^{-2} sr^{-1} cm; emitted radiance per wavenumber interval) is defined as

$$B(\tilde{\nu}, T) = \frac{2h\tilde{\nu}^3 c^2}{e^{hc\tilde{\nu}/k_B T} - 1},$$

where $\tilde{\nu}$ is the standard notation for wavenumber (the inverse of wavelength). With this definition, $\pi B(\tilde{\nu}, T)d\tilde{\nu}$ is the power per area of photons emitted by a blackbody surface with wavenumbers between $\tilde{\nu}$ and $\tilde{\nu} + d\tilde{\nu}$.

The middle panel of Fig. 2 shows the carbon dioxide absorption coefficient κ calculated at a temperature of 289 K and a total atmospheric pressure of 10^5 Pa (1 bar). The 15-μm band, centered at 15 μm (667 cm^{-1}) and defined here to be the wavenumbers between 467 and 867 cm^{-1}, is a prominent feature in the absorption spectrum of carbon dioxide, which is another reason why this band dominates its forcing. At the very center of the band (around 667 cm^{-1}), a meter of dry surface air with today's CO_2 concentration is virtually opaque; at the wings of the band, an entire dry atmospheric column is virtually transparent.

When talking about spectral forcings, we will put a subscript $\tilde{\nu}$ on the forcing variable (e.g., $F_{\tilde{\nu}}^{tot}$ or $F_{\tilde{\nu}}^{2\times}$) to denote that it is the forcing per wavenumber interval. In particular,

---

[2] The cloud-resolving model used for Fig. 1 was Das Atmosphärische Modell (DAM; Romps 2008), which was run to radiative-convective equilibrium (RCE) over a 300-K ocean. In the snapshot from this simulation, the total cloud cover is 35%: looking down from space, 12% of the domain is covered by warm cloud tops (>273.15 K) and 23% by cold cloud tops. The simulation used the Rapid Radiative Transfer Model for general circulation models radiation scheme (RRTMG; Iacono et al. 2008) and a preindustrial CO_2 concentration of 280 parts per million by volume (ppmv). With this CO_2 concentration and radiation scheme, the brightness temperature of the top-of-atmosphere (TOA) upwelling longwave varies spatially from a minimum of 210 K over cumulonimbus anvil clouds to a maximum of 264 K in clear sky (which is far from the surface temperature due, in large part, to the high precipitable water content of this tropical atmosphere).
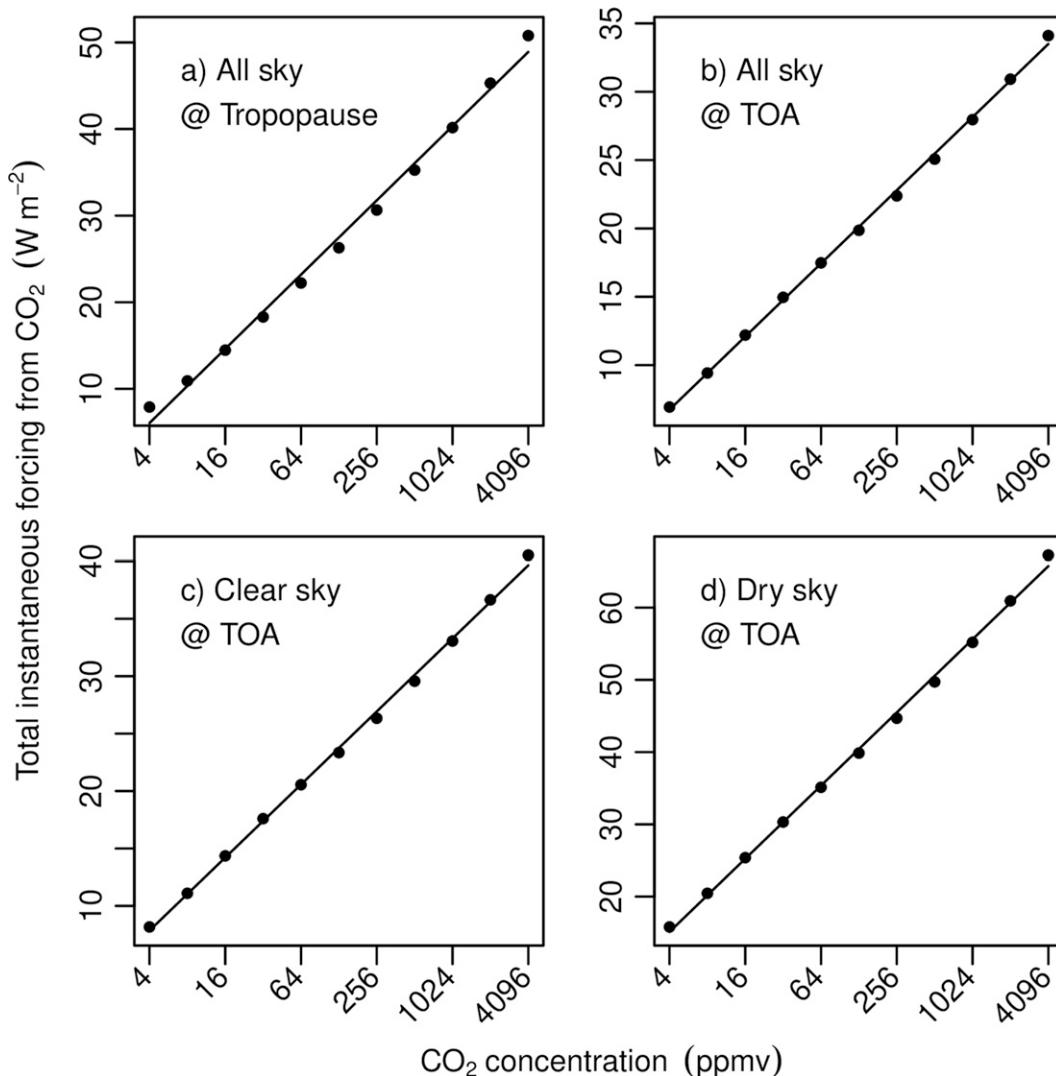
FIG. 1. Total instantaneous forcing F^{tot} calculated using RRTMG in a snapshot of a cloud-resolving RCE simulation plotted as circles for various CO_2 concentrations using (a) tropopause all-sky fluxes, (b) TOA all-sky fluxes, (c) TOA clear-sky fluxes (in which condensates have been zeroed), and (d) TOA dry-sky fluxes (in which condensates and water vapor have been zeroed). The lines are least squares fits. The r^2 values exceed 99% in all cases.

$F_{\tilde{\nu}}^{2\times}(\tilde{\nu},q)d\tilde{\nu}$ is the contribution to $F^{2\times}(q)$ from wavenumbers in $[\tilde{\nu}, \tilde{\nu} + d\tilde{\nu}]$. The top panel of Fig. 2 plots $F_{\tilde{\nu}}^{2\times}(\tilde{\nu}, 256 \text{ ppmv})$ for carbon dioxide (calculated with the line-by-line model) in an idealized atmosphere that we will refer to as IsoStrat because the stratosphere is isothermal. All line-by-line calculations were performed using concentrations that are a power of 2 in parts per million by volume, so 256 ppmv is used here as the closest representative of a preindustrial value of ~280 ppmv. The IsoStrat atmosphere has a 289-K blackbody surface overlain by a troposphere whose temperature drops from 289 K at the 10^5-Pa surface to 205 K at the 10^4-Pa tropopause, which is overlain by a 205-K isothermal stratosphere (see section 4 for a precise definition of IsoStrat and the other atmospheres used in this paper). Since this paper focuses on instantaneous forcings, the model atmospheres used here are static (i.e., they are independent of the greenhouse gas concentrations). As seen from Fig. 2, $F^{2\times}$ from CO_2 at modern concentrations is almost entirely due to changes in upwelling longwave fluxes in the 15-μm band, so that is where we will focus our attention in the sections that follow.

3. The basic mechanism

Consider an atmosphere with a single well-mixed longwave absorber with a volume fraction q and an absorption coefficient κ that depends on wavenumber. Ignoring the pressure and temperature dependence of κ, the optical depth τ (measured from the top of the atmosphere) at some wavenumber at some height in the atmosphere is proportional to three quantities: the overlying air mass (which is proportional to

pressure p), the volume fraction q of the longwave absorber, and the absorption coefficient κ. In other words, $\tau \propto pq\kappa$, where we are using the standard symbol of $\propto$ for proportionality (i.e., if $y = ax$ for some $a \neq 0$, then $y \propto x$). Emission to space occurs from the vicinity of the emission pressure p_{em}, defined to be the pressure in the atmosphere where τ equals one. Therefore, in the proportionality $\tau \propto pq\kappa$, we can set τ to 1 and p to p_{em}, which gives $p_{em} \propto 1/(q\kappa)$. Taking the logarithm[3] of both sides reveals that $\log(p_{em})$ is linear in $\log(q\kappa)$,

$$\log(p_{em}) \sim -\log(q\kappa). \tag{1}$$

We will refer to this below as property 3. Here and throughout, we use the symbol $\sim$ to denote a linear relationship; that is, if $y = ax + b$ for some $a \neq 0$ and $b \neq 0$, then $y \not\propto x$, but $y \sim x$. We have retained a minus sign in relation (1) as a reminder that an increase in $\log(q\kappa)$ pushes the unit optical depth to higher altitudes, leading to a decrease in $\log(p_{em})$. Ignoring the pressure and temperature dependence of κ, relation (1) is true for any atmosphere with a single well-mixed absorber; we will see in section 5d that relation (1) also holds to good approximation when those dependencies are included.

As a visual guide, we will use an analogy to a freight train to describe Earth's radiation to space from within the 15-μm band. In this analogy, the train track runs flat along Earth's surface until it slopes upward through the troposphere and into the stratosphere. The train straddles the troposphere with its head in or near the stratosphere and its tail on the surface. The cargo carried by the train are all the wavenumbers of the 15-μm band, with each train car carrying a same-sized set of those wavenumbers. Furthermore, each car has a spotlight pointing upward, sending infrared radiation directly to space with an intensity that depends on temperature: as a train car climbs upward to colder parts of the atmosphere, its light dims. All of the spotlights dim with ascent in the same way, so moving the train forward by one car has a simple effect on the emission to space: it effectively moves one train car from the warm surface to the cold stratosphere. Finally, if the train moves forward by, say, one train car every time the CO_2 concentration is doubled, then every doubling of CO_2 effectively moves one train car from the surface to the stratosphere, dimming its spotlight accordingly; indeed, we will see that the train moves in this way. What makes this analogy to a freight train particularly apropos is that, like a real freight train, each train car is the same length (there are no short cars or long cars), each car holds the same amount of stuff (in this case, equal-sized sets of wavenumbers), and all the cars move with the same speed.

For CO_2 in an otherwise transparent Earth-like atmosphere, there are five properties that combine to make this train analogy work (i.e., that make the forcing from CO_2 approximately logarithmic in its concentration q for q in the range of 4 to 4096 ppmv). These properties are as follows:

1) For carbon dioxide concentrations of 4 to 4096 ppmv—a range that encompasses all values experienced on Earth
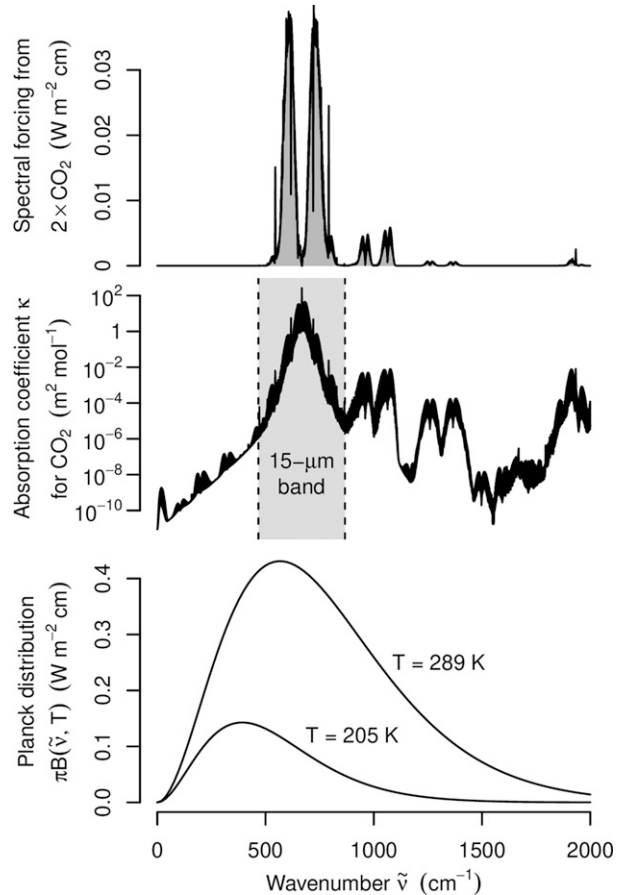

FIG. 2. Functions of wavenumber $\tilde{\nu}$: (top) $F_{\tilde{\nu}}^{2\times}(\tilde{\nu}, 256\,\text{ppmv})$, the spectral forcing, shown here smoothed by a 2 cm^{-1} moving window, caused by a doubling of CO_2 from 256 to 512 ppmv in IsoStrat, a dry atmosphere with a troposphere sandwiched between an isothermal 205-K stratosphere ($p < 10^4$ Pa) and a 289-K surface ($p = 10^5$ Pa); (middle) carbon dioxide absorption coefficient κ calculated at a temperature of 289 K and a total air pressure of 1 bar given in units of m^2 per mole of carbon dioxide molecules; and (bottom) the solid-angle-integrated spectral blackbody Planck emission πB for two different temperatures (205 and 289 K).

within the past 300 million years (Berner 2006) as well as any plausible values for the remainder of the Anthropocene—the forcing from carbon dioxide is dominated by the 15-μm band; this tells us that focusing on our 15-μm "freight train" is warranted.

2) For a given pressure and temperature, the wavenumbers in the 15-μm band are distributed approximately uniformly within an interval of $\log(\kappa)$; this tells us that the train cars hold same-sized sets of wavenumbers.

3) Even when accounting for the pressure and temperature dependencies of κ, $\log(p_{em}) \sim -\log(q\kappa)$ is valid to good approximation [i.e., Eq. (1) still holds]; this tells us that the train cars move together (as they should for a train!) and by how much they move for a given change in the carbon dioxide concentration.
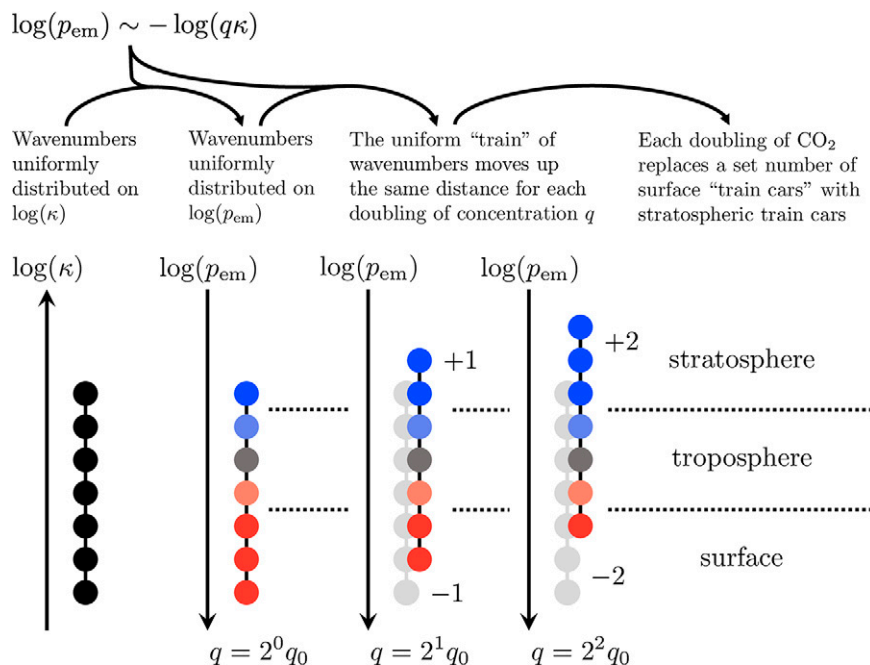
---

[3] Unless given a subscript, all logarithms are natural logarithms, i.e., with base e.

$$\log(p_{\rm em}) \sim -\log(q\kappa)$$

Wavenumbers uniformly distributed on $\log(\kappa)$

Wavenumbers uniformly distributed on $\log(p_{\rm em})$

The uniform "train" of wavenumbers moves up the same distance for each doubling of concentration q

Each doubling of CO_2 replaces a set number of surface "train cars" with stratospheric train cars

$\log(\kappa)$ $\log(p_{\rm em})$ $\log(p_{\rm em})$ $\log(p_{\rm em})$

$+1$ $+2$ stratosphere

troposphere

surface

-1 -2

$q = 2^0 q_0$ $q = 2^1 q_0$ $q = 2^2 q_0$

FIG. 3. Explanation of why the forcing from carbon dioxide is logarithmic in its concentration. Each black circle denotes an equal-sized set of wavenumbers. (first axis) By property 1, we can focus on the 15-μm band, which, by property 2, has its wavenumbers uniformly distributed within an interval of $\log(\kappa)$. (second axis) By property 3, this implies that the wavenumbers are uniformly distributed within an interval of $\log(p_{\rm em})$. Consistent with property 4, the head of the "train" of wavenumbers is in the stratosphere and the rear of the train is in the surface. (third axis) By property 3, $\log(p_{\rm em})$ is linear in $\log(q)$, so multiplying q by successive multiplicative factors (e.g., doublings) moves the train to lower $\log(p_{\rm em})$ by the same amount. Here, a doubling is illustrated as moving the train up by one car. By property 5, the Planck distribution is approximately a function of temperature only, so a set of wavenumbers emitting to space from the warm surface temperature (red colors) has been effectively replaced by an equal-sized set of wavenumbers emitting to space from the cold stratosphere (blue colors). (fourth axis) Another doubling moves another equal-sized set of wavenumbers from the surface to the stratosphere. The size of the set of wavenumbers moved from the surface to the stratosphere is proportional to $\log(q)$, so the forcing is proportional to $\log(q)$. As a visual aid, the light-gray circles mark where the train was for $q = q_0$.

4) For carbon dioxide concentrations ranging from 4 to 4096 ppmv, wavenumbers with the lowest κ in the 15-μm band have an optical depth much less than one at the surface while the wavenumbers with the highest κ have an optical depth of one near the tropopause or in the stratosphere; this tells us that rear of the train is on the surface and the head of the train is in or near the stratosphere.

5) For tropospheric temperatures, 15 μm is where the temperature dependence of the Planck distribution is nearly independent of wavenumber; this tells us that the spotlights all dim in the same way as they ascend.

Figure 3 illustrates how these facts combine to generate the logarithmic forcing of carbon dioxide. By virtue of property 1, we can focus on the 15-μm band, whose wavenumbers have been grouped into seven sets (or "train cars"), schematically represented by the black circles. The wavenumbers could be grouped into many more sets—even an uncountably infinite number—but seven sets are depicted here for simplicity of

illustration.[4] On the left side of Fig. 3, the wavenumbers are shown as uniformly distributed over an interval of $\log(\kappa)$ in accordance with property 2. By property 3, $\log(p_{\rm em})$ is linear in $\log(\kappa)$, so the wavenumbers are also distributed uniformly over an interval of $\log(p_{\rm em})$. (For wavenumbers that have an optical depth less than one at the surface, we can still calculate $p_{\rm em}$ by imagining that we replace the surface with a hydrostatic, semi-infinite atmospheric layer of the same temperature. This has no effect on the radiative fluxes from those wavenumbers above the surface, but it has the benefit of allowing us to visualize how the emission pressures of those wavenumbers approach the surface.) Consistent with property 4, the

---

[4] Each of these seven sets of wavenumbers (or "train cars") can be thought of as the set of spectral intervals that have $\log(\kappa)$ within one of seven non-overlapping ranges. Section 6 gives a more precise definition, which reveals that a train car has contributions from all wavenumbers, but primarily from those with similar $\log(\kappa)$.
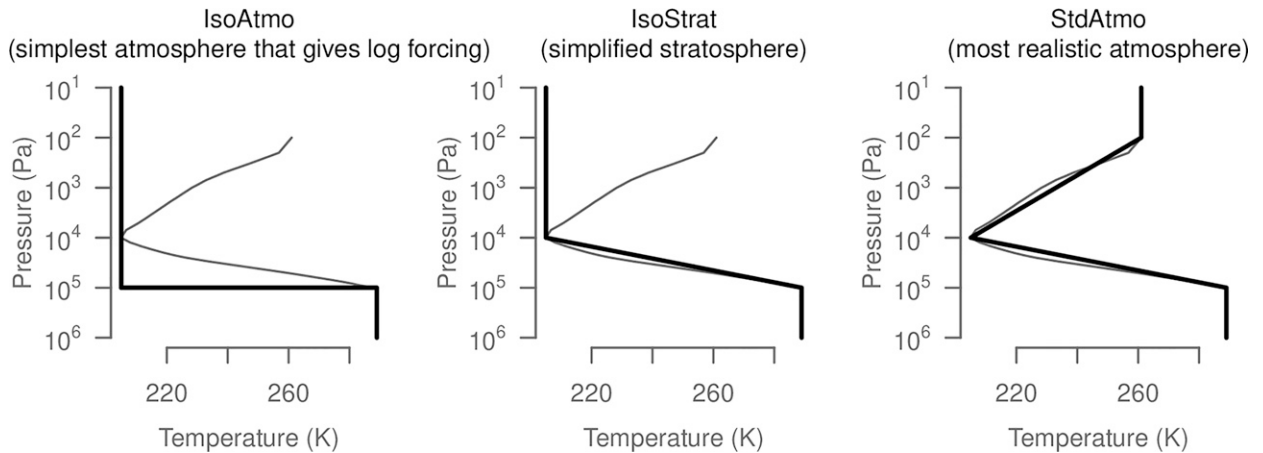
FIG. 4. The temperature profiles of three model atmospheres: (from left to right) IsoAtmo, IsoStrat, and StdAtmo. The area-weighted mean of atmospheric temperature during year 2020 in the ERA5 (gray).

high values of $\log(p_{em})$ are below the surface and the low values of $\log(p_{em})$ are in the stratosphere. By property 3, $\log(p_{em})$ is also linear in $\log(q)$, so *each doubling* of the CO_2 concentration *q* moves the train of wavenumbers to lower $\log(p_{em})$ *by the same amount*. This is depicted in Fig. 3 with one doubling moving the train upward by one car length and two doublings moving the train upward by two car lengths.

We see, therefore, that an increase in the CO_2 concentration has a simple effect: it replaces some number of train cars in the surface with an equal number of train cars in the stratosphere (Pierrehumbert 2010, 2011; Wilson and Gea-Banacloche 2012; Jeevanjee et al. 2021). Since these train cars represent equal-sized sets of wavenumbers emitting to space, this means that a set of wavenumbers emitting to space at the surface temperature has been effectively replaced with an equal-sized set of wavenumbers emitting to space from the stratospheric temperature. Then, using property 5, we can ignore the Planck distribution's explicit dependence on the wavenumber; this makes the Planck distribution a function of temperature only [i.e., $B = B(T)$]. Therefore, wavenumbers emitting to space from the surface are sending to space a spectral flux equal to $\pi B(T_{surf})$ and wavenumbers emitting to space from the stratosphere are sending to space a spectral flux equal to $\pi B(T_{strat})$. If $\Delta\tilde{\nu}$ is the size of the set of wavenumbers effectively moved from the surface to the stratosphere by a doubling of carbon dioxide, the change in forcing from a doubling is

$$F^{2\times} = \pi\big[B(T_{surf}) - B(T_{strat})\big]\Delta\tilde{\nu}.$$

Since every doubling of concentration effectively moves a set of the same size $\Delta\tilde{\nu}$, we get this same added forcing from each doubling. Or, for a more general change in concentration, $\Delta\tilde{\nu} \propto \Delta\log(p_{em}) \sim \Delta\log(q)$, so the total forcing from carbon dioxide is approximately logarithmic in its concentration; that is, $F^{tot} \sim \log(q)$. This holds for concentrations within roughly 4 to 4096 ppmv. For concentrations below 4 ppmv, the head of the train is too close to the surface and so property 4 no longer holds. For concentrations above 4096 ppmv, other bands of CO_2 start to generate substantial forcing

(e.g., Zhong and Haigh 2013) and so property 1 no longer holds.

As we have seen, the derivation of logarithmic forcing hinges on the validity of properties 1 through 5. Section 5 will explore these properties in more detail and show that they hold for carbon dioxide in an Earth-like atmosphere.

4. Model atmospheres

We will describe here the five model atmospheres used throughout the paper. All of the atmospheres are dry, transparent to shortwave radiation, hydrostatically balanced with Earth's gravitational constant, and have temperature profiles that are piecewise linear in the logarithm of pressure. The first three atmospheres are IsoAtmo (a cold isothermal atmosphere sitting on top of a warm surface), IsoStrat (a cold isothermal stratosphere that is separated from the warm surface by a troposphere with an Earth-like lapse rate), and StdAtmo (an atmosphere in which both the troposphere and stratosphere have Earth-like lapse rates).

Figure 4 plots the temperature profiles of those three atmospheres as black curves. The gray curve in each of the panels is the global area-weighted mean of atmospheric temperature during year 2020 in the ERA5 reanalysis (Hersbach et al. 2020), plotted from the surface (at 10^5 Pa), through the cold-point tropopause (at 10^4 Pa), and up to the top of the stratosphere (at 10^2 Pa). Noting that the ordinate is the logarithm of pressure, we see that the global-mean temperature can be approximated as two pieces linear in $\log(p)$ that connect a near-surface air temperature of 289 K, to a tropopause temperature of 205 K, and back up to a stratopause temperature of 261 K.

IsoAtmo, shown in the left panel, places a cold isothermal atmosphere directly on top of the warm surface. Here, as throughout the paper, the surface is represented by a semi-infinite atmospheric layer with the same gas composition as the other layers; this is done purely for the purposes of visualization and has no impact on the radiative fluxes at pressures below 10^5 Pa. In reality, placing a cold isothermal layer

IsoAtmo	IsoStrat	StdAtmo	HotStrat	DeepTrop	x between
205	205	261	289	205	$-\infty$ and -79
				$205+(x+79)$	-79 and 2
		$261-28(x-2)$			2 and 4
	$205+84(x-4)$	$205+84(x-4)$	$205+84(x-4)$		4 and 5
289	289	289	289	289	5 and ∞

FIG. 5. For $x \equiv \log_{10}(p/\text{Pa})$, the temperature (in K) for each atmosphere (columns) within each range of x (rows).

directly on top of a warm isothermal layer would induce vigorous convection, but IsoAtmo is a well-defined atmosphere that will serve an important purpose: it will demonstrate that the logarithmic forcing persists even without a continuously varying temperature profile.

IsoStrat, shown in the middle panel, has a troposphere with a realistic lapse rate, but has a stratosphere that is isothermal. The advantage of this atmosphere is conceptual simplicity: the surface and stratosphere are isothermal, and so the movement of sets of wavenumbers from the surface to the stratosphere has a straightforward radiative effect. Fortunately, this simplicity is largely retained in the real atmosphere because the stratosphere has a mean lapse rate—defined here as $dT/d\log(p)$—whose magnitude is only one-third as large as the troposphere's: $dT/d\log(p)$ is 84 K in the troposphere and -28 K in the stratosphere. Therefore, we will find that the logarithmic nature of the forcing is retained in StdAtmo, which is the atmosphere shown in the right panel of Fig. 4.

These three atmospheres, plus two others, are defined in Fig. 5. The HotStrat and DeepTrop atmospheres are modifications of IsoStrat in which the stratosphere is given the same temperature as the surface (HotStrat) or the troposphere is made much deeper (DeepTrop). HotStrat and DeepTrop will be used in sections 9 and 10.

5. The five properties

a. Property 1: Dominance of the 15-μm band

We saw in the top panel of Fig. 2 that $F^{2\times}(256\ \text{ppmv})$ in IsoStrat is dominated by the 15-μm band. Figure 6 shows, using the line-by-line model, that the 15-μm band dominates over a wide range of CO_2 concentrations in StdAtmo (the most realistic of the model atmospheres). The solid curve shows the fraction of F^{tot} generated by wavenumbers in the 15-μm band (recall that F^{tot} is the TOA upwelling flux without the CO_2 minus the TOA upwelling flux with the CO_2). The dashed curve shows the fraction of $F^{2\times}$ (change in F^{tot} from a doubling of CO_2) that is caused by wavenumbers in the 15-μm band. Since $F^{2\times}(q)$ is defined as the change in forcing from q to $2q$, the value at 2048 ppmv corresponds to doubling from 2048 to 4096 ppmv. We see that, for concentrations ranging from 4 to 4096 ppmv, the 15-μm band is responsible for the majority of the forcing, ranging from 89% to 97% for F^{tot} and from 61% to 98% for $F^{2\times}$. Between 2048 and

4096 ppmv, the bands of CO_2 centered at 15, 10, 7.6, 5, and 4.3 μm contribute 61%, 27%, 6%, 5%, and 1% to $F^{2\times}$, respectively, indicating that bands at shorter wavelengths start to make substantial contributions to the forcing at these large concentrations (Zhong and Haigh 2013). At preindustrial and current concentrations, the 15-μm band is responsible for 96% of F^{tot} and 82%–86% of $F^{2\times}$.

b. Property2: Uniform distribution of log(κ)

The top-left panel of Fig. 7 shows, in the solid curve, the probability distribution function (PDF) of the $\log(\kappa)$ values within the 15-μm band calculated at the surface (1 bar and 289 K) using the line-by-line model. The dashed curve depicts a uniform distribution for illustration. We see that the line-by-line PDF approximates a uniform distribution over a remarkable six orders of magnitude. The bottom-left panel of Fig. 7 shows the corresponding cumulative distribution
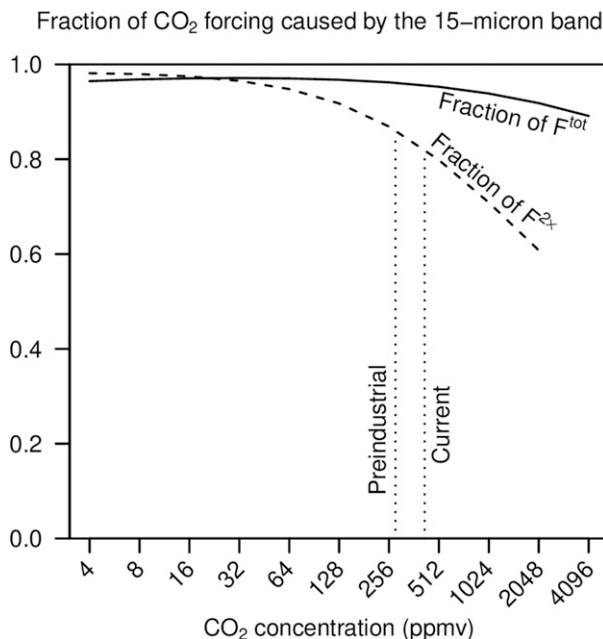

FIG. 6. Fraction of F^{tot} in StdAtmo that is generated by the 15-μm band (solid). Fraction of $F^{2\times}$ in StdAtmo that is generated by the 15-μm band (dashed).
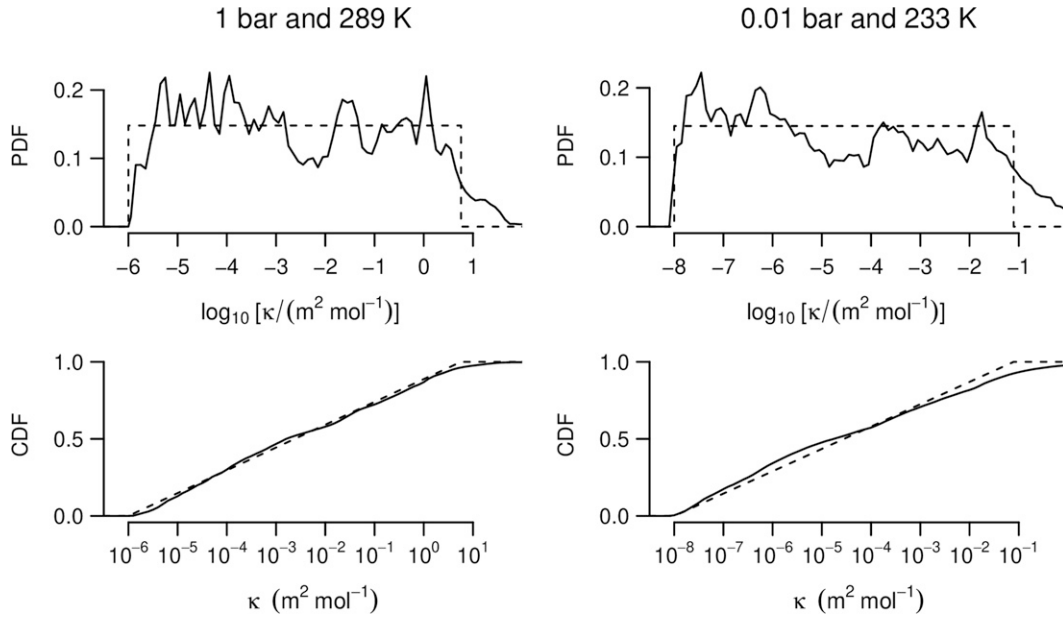
FIG. 7. (top left) Probability distribution function (PDF) of the values of $\log_{10}[\kappa/(m^2 \, mol^{-1})]$ within the 15-μm band calculated at 1 bar and 289 K using the line-by-line model. The dashed curve depicts a uniform distribution for illustration. (bottom left) The corresponding cumulative distribution functions (CDFs). (right) As in the left column, but for 0.01 bar and 233 K (the temperature there in StdAtmo).

function (CDF) of the κ values (i.e., the integral of the PDF). The integral of a uniform distribution, shown by the dashed curve, is an upward-sloping line with values bounded below and above by zero and one, respectively. We see that the line-by-line CDF approximates this closely. The right column plots the PDF and CDF in the stratosphere (0.01 bar and 233 K). Note that the distribution remains approximately uniform, but has shifted to lower κ by a factor equal to the ratio of pressures; this behavior will be explained in section 5c.

The uniform distribution is also apparent when looking at the spectrum as a function of wavenumber. The top-left part of Fig. 8 shows the absorption coefficient $\kappa(\tilde{\nu})$ for the 15-μm band plotted on a log axis and calculated using the line-by-line model at 1 bar and 289 K. Property 2 is apparent from the approximately linear decay of $\log(\kappa)$ as a function of wavenumbers from the center of the band.

Let us now resort those wavenumbers in order of increasing κ, as is done in the k distribution method (e.g., Stephens 1984), which is a standard technique in radiation parameterization. Let the function CDF be the cumulative distribution of κ values within the 15-μm band at this pressure and temperature, which was shown in the bottom-left panel of Fig. 7. In other words, $\text{CDF}(\kappa)$ is the fraction of the 400-cm^{-1}-wide interval of wavenumbers that have an absorption coefficient less than κ. The inverse of this, CDF^{-1}, maps the interval [0, 1] to absorption coefficients in a monotonically increasing way. We can then define $\kappa'(\tilde{\nu})$ as

$$\kappa'(\tilde{\nu}) = \text{CDF}^{-1}\left(\frac{\tilde{\nu} - \tilde{\nu}_1}{\tilde{\nu}_2 - \tilde{\nu}_1}\right), \qquad (2)$$

where $\tilde{\nu}_1 = 467 \, cm^{-1}$ and $\tilde{\nu}_2 = 867 \, cm^{-1}$ are the boundaries of the 15-μm band. By construction, this function is simply a resorting of the original absorption coefficients. It is plotted as the dashed curve in Fig. 8, and it is nothing more than the curve in the bottom panel of Fig. 7 with the axes swapped. Note that $\log(\kappa')$ is nearly linear in wavenumber.

The lower-left part of Fig. 8 plots the Planck distribution within the 15-μm band at temperatures of 205 and 289 K. We see that the *difference* between the two Planck distributions is nearly independent of wavenumber, consistent with property 5. Section 5f will show that this is sufficient for us to ignore the wavenumber dependence of the Planck distribution for the purposes of understanding the forcing. Once this approximation is made, the only physical property that depends on wavenumber is κ. Therefore, we are free to resort the wavenumbers so long as we keep track of the corresponding κ values. In particular, we can replace κ with κ' in calculations of the forcing without affecting the answer.

To go a step further, we can approximate the spectrum shown in the left panel of Fig. 8 with the κ shown in the right panel. This represents $\kappa(p_0, \tilde{\nu})$ at $p_0 = 10^5$ Pa and it is written mathematically as

$$\kappa(p_0, \tilde{\nu}) = \begin{cases} \kappa_0 e^{b\tilde{\nu}} & \tilde{\nu}_1 < \tilde{\nu} < \tilde{\nu}_2 \\ 0 & \text{otherwise}, \end{cases} \qquad (3)$$

with $\tilde{\nu}_1 = 467 \, cm^{-1}$ and $\tilde{\nu}_2 = 867 \, cm^{-1}$. Fitting Eq. (3) to the κ' in the left panel using least squares, we find best-fit coefficients of $\kappa_0 = 8.4 \times 10^{-15} \, m^2 \, mol^{-1}$ and $b = 0.04$ cm. Equation (3) is nearly all of the spectroscopic information that is needed to construct a model of the forcing from carbon
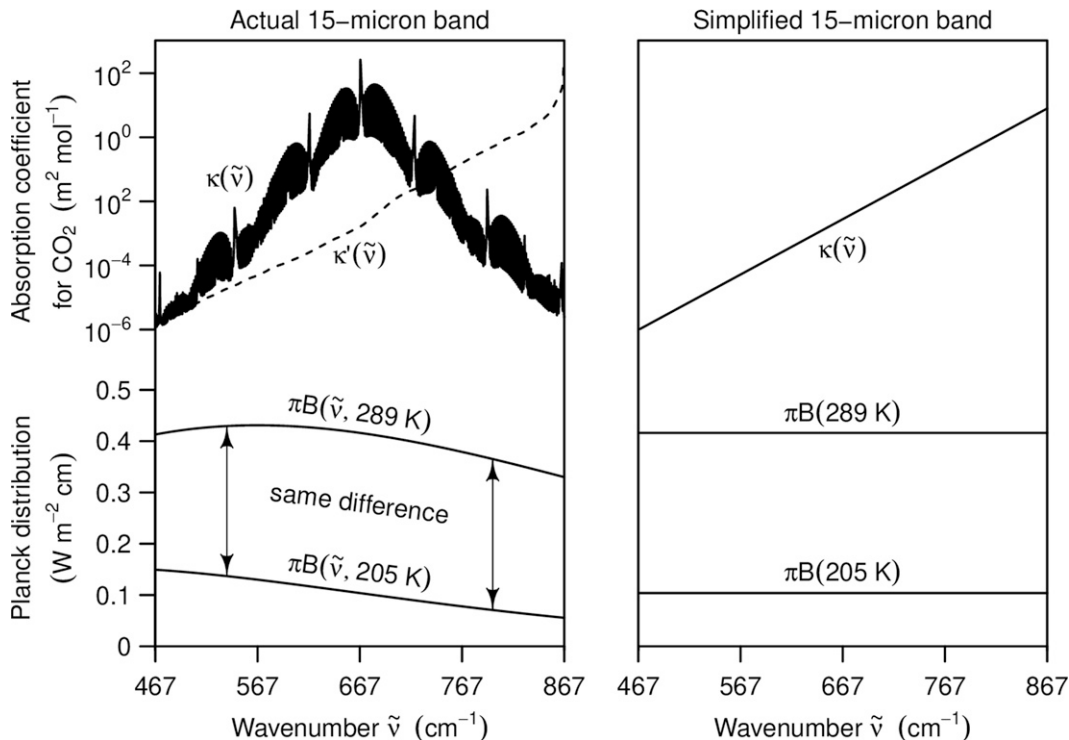
FIG. 8. (top left) Plots of the absorption coefficient $\kappa(\tilde{\nu})$ of carbon dioxide at 1 bar and 289 K (solid) and the resorted $\kappa'(\tilde{\nu})$ defined in Eq. (2) (dashed). (bottom left) The Planck distributions at temperatures of 205 and 289 K. (top right) The simple model's absorption coefficient $\kappa(\tilde{\nu})$, which is exponential in $\tilde{\nu}$. (bottom right) The simple model's Planck distributions, which have no explicit dependence on wavenumber.

dioxide. The only remaining detail is to specify how κ varies with pressure.

c. Linearity of κ in pressure

In section 3, we ignored any pressure or temperature dependence of κ when we derived relation (1). We will now show that relation (1) continues to hold even with those dependencies.

The value of κ at any particular wavenumber has contributions from spectral lines representing many different vibrational and rotational transitions of CO_2, and each of those lines has a shape that varies with temperature and pressure. To get an indication of how this sum of contributions might change with pressure and temperature, we can use the Lorentz line shape. The Lorentz line shape can be derived from first principles with some approximations (e.g., Van Vleck and Weisskopf 1945) and is supported empirically within about 100 line widths of the line center (Pierrehumbert 2010). Although line-by-line models use a line shape that deviates from this, especially far from the line center, the Lorentz line shape is adequate for our discussion here.

With a Lorentz line shape, the absorption coefficient due to a single line centered at $\tilde{\nu}_c$ is

$$\kappa = \frac{S(T)}{\pi\gamma} \frac{\gamma^2}{\gamma^2 + (\tilde{\nu} - \tilde{\nu}_c)^2},$$

where the line width γ can be represented by

$$\gamma = \gamma_0 \frac{p}{p_0}\left(\frac{T_0}{T}\right)^n$$

with an n that varies from line to line but is typically around 0.5 (Pierrehumbert 2010). This line shape is plotted in the left panel of Fig. 9 using $\gamma = 0.1$ cm^{-1}.

Although both the line intensity S and line width γ depend on temperature, it is the dependence of γ on pressure that tends to dominate the changes in line shapes as we move up and down in the atmosphere (Pierrehumbert 2010). Far from the line center ($\tilde{\nu} - \tilde{\nu}_c \gg \gamma$), when pressure is varied isothermally, κ varies linearly with pressure. The right panel of Fig. 9 plots $\partial\log(\kappa)/\partial\log(p)$ to illustrate this point: everywhere except for the vicinity of the line center, this derivative is unity, indicating a proportionality with respect to pressure.

To the extent that the prominent spectral lines of CO_2 are sufficiently well spaced, this result tells us that most of the 15-μm band should scale linearly with pressure. Thus, it might be sufficient to approximate κ as linear in pressure throughout the entire band. It is not obvious a priori that this should work since there are also temperature dependencies of the individual line shapes and line strengths, but it does work in many cases and it is a common approximation (Pierrehumbert 2010). To demonstrate the approximate linearity in pressure,
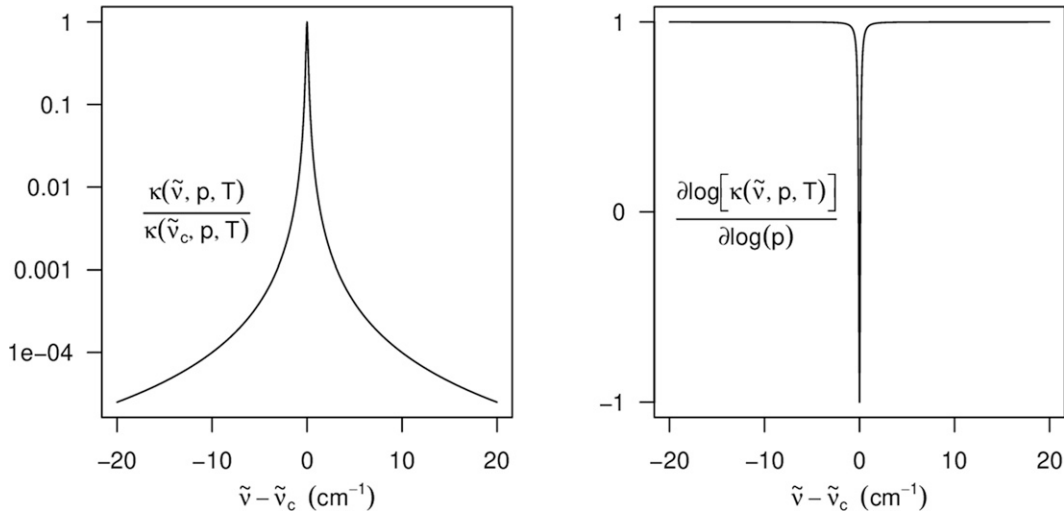
FIG. 9. (left) Absorption coefficient κ for a single spectral line with a Lorentz line shape with width $\gamma = 0.1$ cm^{-1}. The absorption coefficient is plotted as a function of distance (in wavenumber) from the line center, and it is plotted as normalized by the value at line center. (right) The change in $\log(\kappa)$ for this spectral line per change in $\log(p)$, keeping temperature constant. Where the value is one, κ scales linearly with pressure.

Fig. 10 plots κ calculated from the line-by-line model as a function of pressure level for 4000 equally spaced wavenumbers in each of three different atmospheres (IsoAtmo, IsoStrat, and StdAtmo). To avoid the figures becoming saturated with color, the individual curves are plotted using a translucent color. We see that, regardless of the thermal structure of the atmosphere, the vast majority of the wavenumbers have κ values that increase quasi-linearly as we move to higher pressure in the atmosphere. The lower-right panel quantifies this by plotting three histograms (one for each atmosphere) of the slopes of the best-fit lines to each of the 4000 curves. Less than 2% (1%, 3%) of the slopes in IsoAtmo (IsoStrat, StdAtmo) case are negative. We see that the slopes are clumped around unity, demonstrating the quasi-linear dependence of κ on pressure.

Since the κ values are approximately linear in p, we can generalize Eq. (3) to give a simplified model for κ at any pressure:

$$\kappa(p,\tilde{\nu}) = \begin{cases} \dfrac{p}{p_0}\,\kappa_0 e^{b\tilde{\nu}} & \tilde{\nu}_1 < \tilde{\nu} < \tilde{\nu}_2 \\ 0 & \text{otherwise.} \end{cases} \qquad (4)$$

This equation, together with the constants given at the end of section 5b, is all of the spectroscopic information we need about carbon dioxide to understand its forcing for concentrations in the range of 4 to 4096 ppmv.

d. Property 3: $\log(p_{em}) \sim -\log(q\kappa)$

Now that we have this simple model for κ, it is straightforward to reassess the validity of relation (1). For a single well-mixed greenhouse gas, the longwave optical depth is defined as

$$\tau(p,\tilde{\nu},q) = \int_0^p \frac{dp}{gm_0} fq\kappa. \qquad (5)$$

Here, g is the gravitational acceleration (9.81 m s^{-2}), dp/g is the differential overlying air mass per area, q is the volume fraction of the greenhouse gas (e.g., 256 ppmv), κ is the absorption coefficient (i.e., the absorption cross section per molecule), m_0 is the mean mass per molecule of air (29 g mol^{-1}), and $f = 5/3$ is the diffusivity factor used to approximate an integration over the hemisphere of propagation directions (Elsasser 1942). Substituting the expression for κ from Eq. (4), this gives

$$\tau(p,\tilde{\nu},q) = \begin{cases} \dfrac{fp^2 q\kappa_0}{2gp_0 m_0}\,e^{b\tilde{\nu}} & \tilde{\nu}_1 < \tilde{\nu} < \tilde{\nu}_2 \\ 0 & \text{otherwise.} \end{cases} \qquad (6)$$

As before, we can define the emission pressure p_{em} as the pressure level where $\tau = 1$. Setting τ to one in Eq. (6) and solving for pressure, we get

$$p_{em}(\tilde{\nu},q) = \begin{cases} \sqrt{\dfrac{2gp_0 m_0}{fq\kappa_0}}\,e^{-b\tilde{\nu}/2} & \tilde{\nu}_1 < \tilde{\nu} < \tilde{\nu}_2 \\ \infty & \text{otherwise.} \end{cases} \qquad (7)$$

Here, an infinite $p_{em}(\tilde{\nu},q)$ means that the emission to space at wavenumber $\tilde{\nu}$ emanates from the surface regardless of q; recall that, in this simple model, carbon dioxide has no absorptivity outside of $\tilde{\nu}_1$ to $\tilde{\nu}_2$. Using Eq. (4), we can write Eq. (7) as $p_{em} = \sqrt{2gp_0 m_0/fq\kappa(p_0,\tilde{\nu})}$. Taking the logarithm of this, we find that we recover property 3, which states that $\log(p_{em}) \sim -\log(q\kappa)$, so long as we interpret the term κ in this linear relation as being evaluated at some reference pressure.

e. Property 4: Head in the stratosphere and rear in the surface

With Eq. (7), we can evaluate whether property 4 is true, that is, if the head of the wavenumber train is in or near the
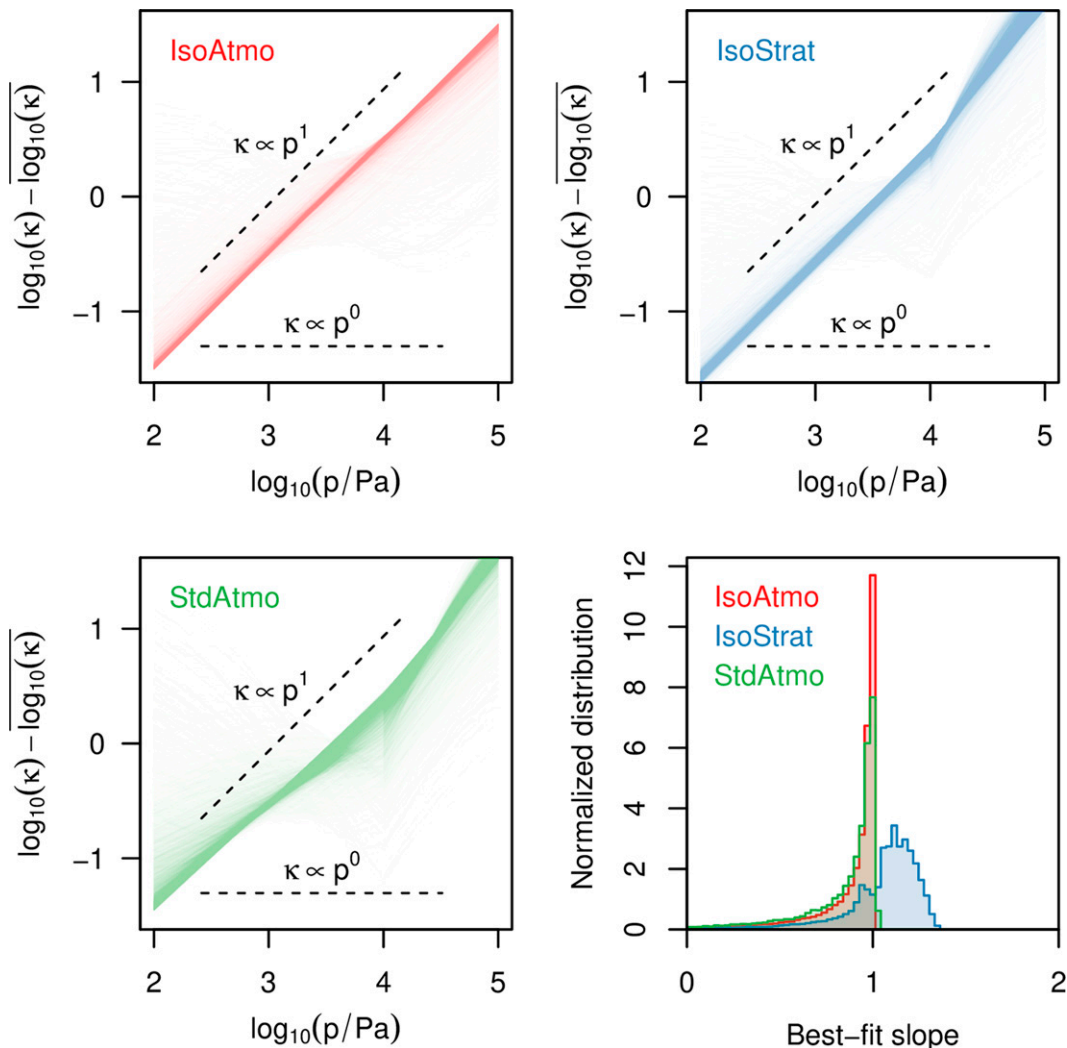
FIG. 10. Translucent plots of $\kappa[\tilde{\nu}, p, T(p)]$ as a function of p for 4000 equally spaced samples of $\tilde{\nu}$ from 467 to 867 cm^{-1} for the (top left) IsoAtmo, (top right) IsoStrat, and (bottom left) StdAtmo atmosphere. The bar in $\overline{\log_{10}(\kappa)}$ represents an average over $\log_{10}(p/\text{Pa})$ from 2 to 5. (bottom right) For each case, the histogram of the best-fit slopes for each of the 4000 wavenumbers.

stratosphere and if the rear of the wavenumber train is in the surface. Using the values for b and κ_0 obtained in section 5b, we can calculate the minimum and maximum emission pressures from Eq. (7) as $p_{em}(\tilde{\nu}_2, q)$ and $p_{em}(\tilde{\nu}_1, q)$, which correspond to the head and rear of the train, respectively. Figure 11 plots these as functions of q from 4 to 4096 ppmv. At all of these concentrations, the rear is in the surface. At modern concentrations, the head is in the stratosphere. At 4 ppmv, the head of the train is in the upper troposphere at 300 mbar, but we will see in section 7 that this is close enough to the tropopause to make $F^{2\times}$ nearly as large (75% as big) as it is when the head of the train is well ensconced in the stratosphere.

Only those wavenumbers emitting to space from above the surface contribute to F^{tot}. Those are the wavenumbers whose $\kappa(p_0, \tilde{\nu})$ exceeds $2gm_0/fqp_0$. For $q = 4$ (256, 4096) ppmv, these

are the wavenumbers with $\kappa(p_0, \tilde{\nu})$ exceeding 0.9 (0.01, 8 × 10^{-4}) m^2 mol^{-1}. The middle panel of Fig. 2 can be used to identify the wavenumbers in the original (unsorted) spectral space that contribute to F^{tot} at each of these concentrations.

f. Property 5: Wavenumber independence of the Planck distribution

If we approximate all of a wavenumber's radiation to space as coming from its emission pressure, then the spectral forcing from a doubling of concentration is

$$F_{\tilde{\nu}}^{2\times}(\tilde{\nu}, q) \approx \pi B\{\tilde{\nu}, T[p_{em}(\tilde{\nu}, q)]\} - \pi B\{\tilde{\nu}, T[p_{em}(\tilde{\nu}, 2q)]\}. \quad (8)$$

We see that $F_{\tilde{\nu}}^{2\times}$ does not depend on the overall magnitude of B, but on how much it changes with respect to temperature.
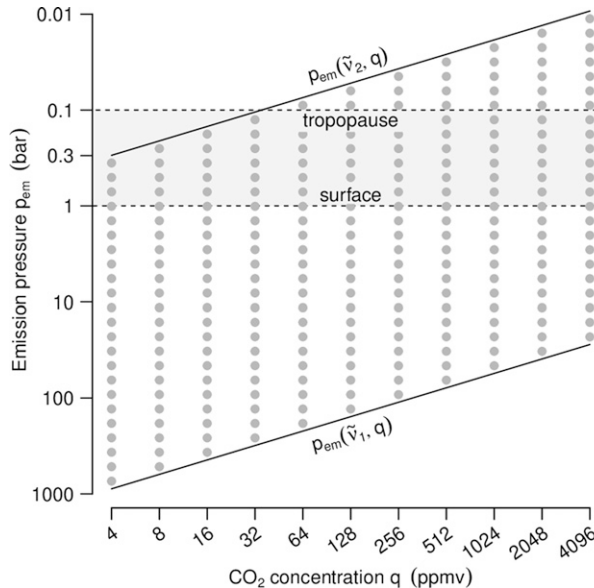
FIG. 11. The locations of the train's head and rear, $p_{em}(\tilde{\nu}_2, q)$ and $p_{em}(\tilde{\nu}_1, q)$, as functions of the CO_2 concentration q.
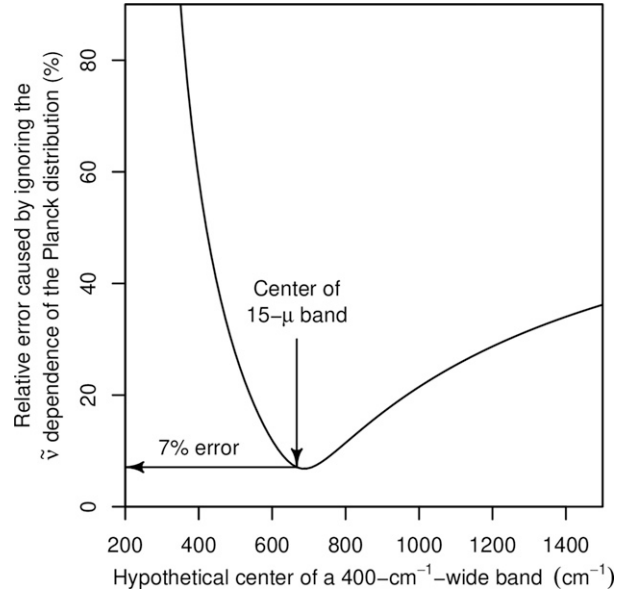

FIG. 12. Error [RMSRE from Eq. (9)] produced by ignoring the explicit wavenumber dependence of the Planck distribution, plotted as a function of the center of a hypothetical 400 cm^{-1}-wide band. The 15-μm band of carbon dioxide is located close to where this error is minimized.

Likewise, $F^{2\times}$, which is simply an integral of $F_{\tilde{\nu}}^{2\times}$, depends only on how B changes with temperature and not its overall magnitude. Therefore, if the change in B with temperature is independent of the wavenumber to good approximation, then we can approximate B as having no explicit dependence on wavenumber (as was depicted in the right column of Fig. 8).

In Earth's troposphere, the globally averaged temperatures range from 205 to 289 K. We need to know, therefore, whether $B(\tilde{\nu}, 289\,\text{K}) - B(\tilde{\nu}, 205\,\text{K})$, for the various $\tilde{\nu}$ within the band, can be approximated as $B(\tilde{\nu}_0, 289\,\text{K}) - B(\tilde{\nu}_0, 205\,\text{K})$, where $\tilde{\nu}_0$ is the wavenumber in the middle of the band. For this to be true, we would need dB/dT at the midtropospheric temperature of 247 K (the average of 205 and 289 K) to be independent of $\tilde{\nu}$ in the vicinity of $\tilde{\nu} = \tilde{\nu}_0$. In other words, we would need $d^2B/dT\,d\tilde{\nu} = 0$ at $T = 247$ K and $\tilde{\nu} = 1/(15\,\mu\text{m}) = 667\,\text{cm}^{-1}$. By differentiation of the Planck distribution, we find that $d^2B/dT\,d\tilde{\nu} = 0$ when $\tilde{\nu} = xkT/hc$, where x is the solution to $x = 4(1 - e^{-x})/(1 + e^{-x})$, which evaluates to $x \approx 3.83$. For the midtropospheric temperature of $T = 247$ K, this gives $\tilde{\nu} = 658\,\text{cm}^{-1} = 1/(15.2\,\mu\text{m})$, confirming that the 15-μm band is ideally situated for property 5 to be valid.

We can also check property 5 numerically. For any particular wavenumber $\tilde{\nu}$ in the band, the relative error (RE) caused by ignoring the wavenumber dependence of B is

$$\text{RE} = \frac{B(\tilde{\nu}_0, 289\,\text{K}) - B(\tilde{\nu}_0, 205\,\text{K})}{B(\tilde{\nu}, 289\,\text{K}) - B(\tilde{\nu}, 205\,\text{K})} - 1.$$

For a band that is 400 cm^{-1} wide like the 15-μm band of CO_2, the root-mean-square (RMS) of this relative error (RMSRE) across all the wavenumbers in the band is

$$\text{RMSRE} = \sqrt{\frac{1}{400\,\text{cm}^{-1}} \int_{\tilde{\nu}_0 - 200\,\text{cm}^{-1}}^{\tilde{\nu}_0 + 200\,\text{cm}^{-1}} d\tilde{\nu} \left[\frac{B(\tilde{\nu}_0, 289\,\text{K}) - B(\tilde{\nu}_0, 205\,\text{K})}{B(\tilde{\nu}, 289\,\text{K}) - B(\tilde{\nu}, 205\,\text{K})} - 1 \right]^2}.$$

(9)

This RMSRE is plotted in Fig. 12 as a function of $\tilde{\nu}_0$. We see that the center of the 15-μm CO_2 band is located almost exactly where the RMSRE is minimized. For the 15-μm band, replacing $\tilde{\nu}$ with $\tilde{\nu}_0 = 667 \text{ cm}^{-1}$ in the Planck distribution generates a root-mean-square relative error of only 7%. Since the purpose of this paper is understanding the origin of carbon dioxide's logarithmic forcing, this error is perfectly acceptable. In recognition of property 5, we will henceforth write the Planck distribution as a function only of temperature [i.e., as $B(T)$] with the understanding that it is evaluated at a wavenumber of $\tilde{\nu}_0 = 667 \text{ cm}^{-1}$, that is,

$$B = B(T) = \frac{2h\tilde{\nu}_0^3 c^2}{e^{hc\tilde{\nu}_0/k_B T} - 1}.$$

(10)

6. The log(p) axis

To visualize a greenhouse gas's radiative forcing, we need to derive the weighting function for emission to space, but, to do that, we must first choose an appropriate vertical axis. We learned in section 3 that, by virtue of relation (1) and the particular spectrum of CO_2, the wavenumbers in the 15-μm band are uniformly distributed within an interval of $\log(p_{em})$. This suggests that the most natural vertical coordinate for understanding the radiative forcing from carbon dioxide is

not pressure p or height z, but the logarithm of pressure $\log(p)$. In fact, the case for using $\log(p)$ as the vertical coordinate goes even deeper: not only is it natural to use for CO_2, but the $\log(p)$ axis is also a natural vertical axis to use for any generic greenhouse gas with $\kappa \propto p$.

To see why, note that the spectral flux to space of infrared radiation can be written as

$$\text{Spectral flux to space} = \int_0^\infty \pi B e^{-\tau}\, d\tau. \qquad (11)$$

From the expression for τ in Eq. (5), we know that $\tau \propto p^2$ so long as $\kappa \propto p$. This then implies that $d\tau = 2\tau d\log(p)$. This relation allows us to transform the expression in Eq. (11) from an integral over τ to an integral over $\log(p)$:

$$\text{Spectral flux to space} = \int_{-\infty}^\infty \pi B \underbrace{2e^{-\tau}\tau}_{\equiv \phi_{\log(p)}}\, d\log(p), \qquad (12)$$

where we see that

$$\phi_{\log(p)}(\tilde{\nu}, p, q) \equiv 2e^{-\tau}\tau \qquad (13)$$

is the spectral weighting function for emission to space *on the axis of* $\log(p)$. In other words, $\phi_{\log(p)}(\tilde{\nu}, p, q) d\log(p)$ is the fraction of emission to space at wavenumber $\tilde{\nu}$ that emanates from between $\log(p)$ and $\log(p) + d\log(p)$. Integrating $\phi_{\log(p)}$ over all $\log(p)$ gives a value of one: this can be checked by noting that $\phi_{\log(p)} d\log(p) = e^{-\tau} d\tau$. Figure 13 plots $\phi_{\log(p)}$ for several different concentrations q that all differ by factors of 2. Note that Fig. 13 is not specific to carbon dioxide: it applies to any atmosphere with a single well-mixed greenhouse gas whose absorption coefficients are proportional to pressure.

Since $\phi_{\log(p)}$ is a function only of τ, and since $\tau \propto qp^2$, we can conclude that $\phi_{\log(p)}$ satisfies the following identity:

$$\phi_{\log(p)}(\tilde{\nu}, p, q') = \phi_{\log(p)}\left(\tilde{\nu}, p\sqrt{q'/q}, q\right). \qquad (14)$$

When plotted on a $\log(p)$ axis, this means that an increase in gas concentration from q to q' preserves the shape of $\phi_{\log(p)}$ and simply moves it down the $\log(p)$ axis a distance of $\log(q'/q)/2$. For example, a doubling of the greenhouse gas concentration moves the emission to space to lower $\log(p)$ by an amount $\log(2)/2$; this behavior is evident in Fig. 13. These same properties also carry over to the broadband weighting function for emission to space $\psi_{\log(p)}$, defined as

$$\psi_{\log(p)}(p, q) = \int_0^\infty d\tilde{\nu}\, \phi_{\log(p)}(\tilde{\nu}, p, q). \qquad (15)$$

This is the "train" of emission to space that was alluded to in section 3, where each $\psi_{\log(p)}(p, q) d\log(p)$ (with dimensions of inverse length) can be thought of as a car of that train. Since individual wavenumbers emit to space not just from p_{em}, but from all pressures [with weights given by $\phi_{\log(p)}$], we see now that each train car has contributions from *all* wavenumbers, although it is those wavenumbers with p_{em} near p that contribute most to $\psi_{\log(p)}(p, q) d\log(p)$.
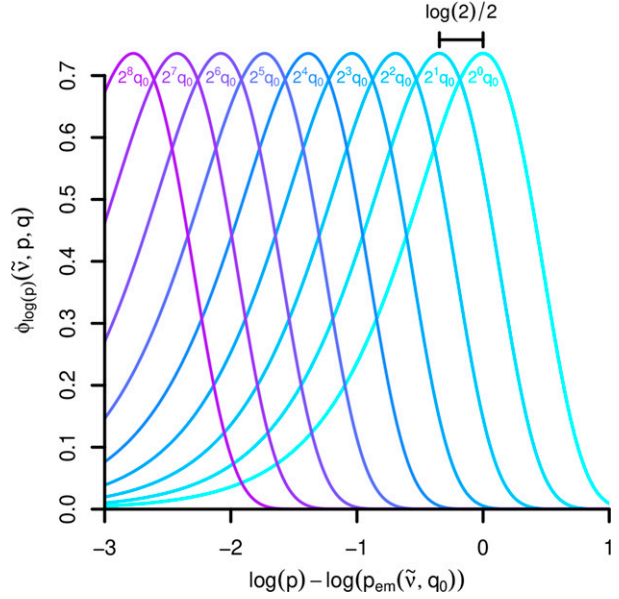

FIG. 13. Weighting function $\phi_{\log(p)}(\tilde{\nu}, p, q)$ of emission to space for any atmosphere with a single well-mixed greenhouse gas whose absorption coefficients are proportional to pressure. The rightmost curve has $q = q_0$ and so peaks where $\log(p) = \log[p_{em}(\tilde{\nu}, q_0)]$. Curves for eight other values of q are also plotted with the value of q labeled just under the peak of each curve.

If we were to use a different vertical coordinate $f(p) \not\propto \log(p)$, such as $f(p) = p$, then the spectral weighting function on the $f(p)$ axis $\phi_{f(p)}$ would be related to $\phi_{\log(p)}$ by

$$\phi_{f(p)}(\tilde{\nu}, p, q) = \frac{d\log(p)}{df(p)} \phi_{\log(p)}(\tilde{\nu}, p, q).$$

Since the factor $d\log(p)/df(p)$ is a function of $p \neq \tau$, $\phi_{f(p)}$ cannot be written as a function solely of τ, and so it does not obey the identity given in Eq. (14). Therefore, a change in q is not equivalent to shifting $\phi_{f(p)}$ down the $f(p)$ axis. Thus, $\log(p)$ is the natural vertical axis for simple models of radiative transfer that approximate κ as either $\kappa = (p/p_0)\kappa(p_0, \tilde{\nu})$, as done above, or as $\kappa = \kappa(\tilde{\nu})$.[5] Fortunately, since $\log(p)$ is approximately proportional to the geometric height z, this is also a somewhat intuitive vertical axis. The $\log(p)$ axis will be used exclusively throughout the remainder of this paper, so we will henceforth drop the subscript $\log(p)$ from weighting functions for notational simplicity.

7. Simple model of the forcing

We now have the pieces we need to derive an analytic expression for the forcing from carbon dioxide. Noting that τ is proportional to p^2, and that $\tau = 1$ when $p = p_{em}(\tilde{\nu}, q)$, we can write τ as

---

[5] When κ is independent of pressure, a change in concentration from q to q' moves ψ down the $\log(p)$ axis by an amount $\log(q'/q)$ instead of $\log(q'/q)/2$.

$$\tau(\tilde{\nu}, p, q) = \frac{p^2}{p_{em}(\tilde{\nu}, q)^2}. \qquad (16)$$

As we learned in the previous section, the spectral weighting function ϕ is $2e^{-\tau}\tau$. Therefore,

$$\phi(\tilde{\nu}, p, q) = 2\exp\left[-\frac{p^2}{p_{em}(\tilde{\nu}, q)^2}\right]\frac{p^2}{p_{em}(\tilde{\nu}, q)^2}. \qquad (17)$$

This applies to any atmosphere with a sole greenhouse gas whose κ scales like p.

To calculate the broadband weighting function ψ, we need to know the details of the function $p_{em}(\tilde{\nu}, q)$. In our simple model of carbon dioxide, $p_{em}(\tilde{\nu}, q)$ takes the form of Eq. (7), which encodes the fact that the wavenumbers of carbon dioxide's 15-μm band have a uniform distribution on $\log(\kappa)$. Using Eqs. (7), (15), and (17) to calculate ψ (see the appendix for details), we get

$$\psi(p, q) = \frac{2}{b}\left[e^{-p^2/p_{em}(\tilde{\nu}_1, q)^2} - e^{-p^2/p_{em}(\tilde{\nu}_2, q)^2}\right]. \qquad (18)$$

This is plotted in Fig. 14 for $q = 256$ ppmv as the curve labeled by $n = 2$. Note that the magnitude of ψ is $2/b = 50$ cm^{-1}. Mathematically, Eq. (18) is closely related to a boxcar function: if the exponents of 2 are replaced with an integer n that is then taken to infinity, we obtain a boxcar function, that is,

$$\lim_{n\to\infty}\left[e^{-p^n/p_{em}(\tilde{\nu}_1, q)^n} - e^{-p^n/p_{em}(\tilde{\nu}_2, q)^n}\right]$$
$$= \begin{cases} 1 & p_{em}(\tilde{\nu}_2, q) < p < p_{em}(\tilde{\nu}_1, q) \\ 0 & \text{otherwise.} \end{cases} \qquad (19)$$

The same boxcar function for ψ would be obtained if the factors of 2 in Eq. (17) for ϕ were replaced with n and taken to infinity; in that limit, $\phi(\tilde{\nu}, p, q) = \delta\{\log(p) - \log[p_{em}(\tilde{\nu}, q)]\}$ and wavenumbers emit to space exactly from their p_{em}. As is evident from Fig. 14, the $n = \infty$ boxcar limit is a decent approximation for the real $n = 2$ case, at least for the purposes of understanding the behavior of the forcing and its overall magnitude.

The total forcing F^{tot} is the integral of $d\log(p)\psi(p, q)$ times the difference between πB at the surface temperature (which is the spectral flux emitted to space if $q = 0$) and πB at the temperature $T(p)$. Mathematically, this is

$$F^{tot}(q) = \int_0^\infty d\log(p)\psi(p, q)\pi\{B(T_{surf}) - B[T(p)]\}. \qquad (20)$$

If we use the boxcar approximation, this becomes

$$F^{tot}(q) \approx 400\,\text{cm}^{-1}\,\pi B(T_{surf})$$
$$- \frac{2\pi}{b}\int_{\log[p_{em}(\tilde{\nu}_2, q)]}^{\log[p_{em}(\tilde{\nu}_1, q)]} d\log(p)B[T(p)]. \qquad (21)$$

Note that this depends on q only through the limits of integration, and a change in $\log(q)$ of $d\log(q)$ changes both limits by $-d\log(q)/2$ (because $p_{em} \propto q^{-1/2}$). Therefore,
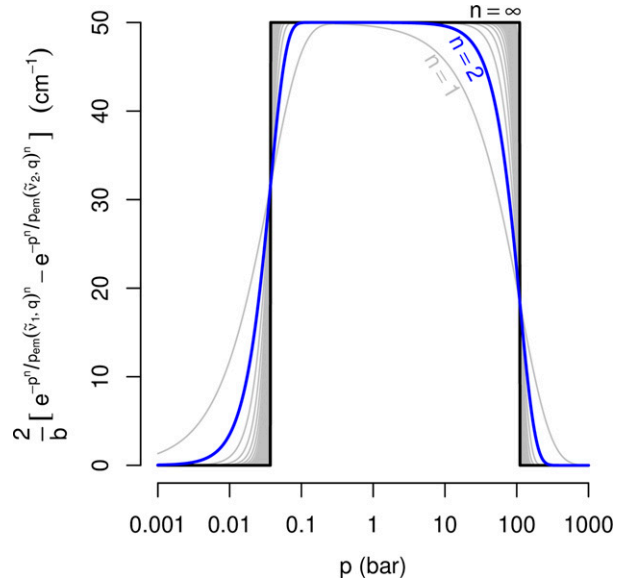

FIG. 14. Plot of ψ, the broadband weighting function for emission to space, from Eq. (18) (blue). Plots of Eq. (18) with the exponents of 2 replaced with other positive integers (gray). Plot of Eq. (18) with the exponents of 2 replaced with ∞ (black).

$$\frac{dF^{tot}}{d\log(q)} \approx \frac{\pi}{b}\left[B\{T[p_{em}(\tilde{\nu}_1, q)]\} - B\{T[p_{em}(\tilde{\nu}_2, q)]\}\right]. \qquad (22)$$

The change in forcing for a doubling is approximately equal to this derivative times $\log(2)$, that is,

$$F^{2\times} \approx \frac{\pi\log(2)}{b}\left[B\{T[p_{em}(\tilde{\nu}_1, q)]\} - B\{T[p_{em}(\tilde{\nu}_2, q)]\}\right]. \qquad (23)$$

If the stratosphere is isothermal and if, as q changes, $p_{em}(\tilde{\nu}_2, q)$ remains greater than the surface pressure and $p_{em}(\tilde{\nu}_1, q)$ remains within the stratosphere, then the two Planck terms will be constant, giving

$$F^{2\times} \approx \frac{\pi\log(2)}{b}\left[B(T_{surf}) - B(T_{strat})\right] \approx 5\,\text{W m}^{-2}. \qquad (24)$$

In this regime, the forcing from a doubling of CO_2 is independent of concentration; this is the well-known logarithmic dependence of forcing on the concentration of CO_2.

While the boxcar approximation is appealing for its simplicity, the forcing is also straightforward to calculate when using the more accurate expression for ψ in Eq. (18). The first panel of Fig. 15 plots this ψ for CO_2 concentrations of 256 (cyan), 512, 1024, and 2048 ppmv (purple) using the values of b and κ_0 found in section 5b. As expected, ψ retains its shape and moves to lower $\log(p)$ by an amount $\log(2)/2$ for each doubling of concentration. The second panel of Fig. 15 plots the temperature profile of the IsoStrat atmosphere.

To visualize where in the atmosphere the forcing is being generated, note that we can write Eq. (20) as $F^{tot} = \int_0^\infty d\log(p)F_{\log(p)}^{tot}(p, q)$, where
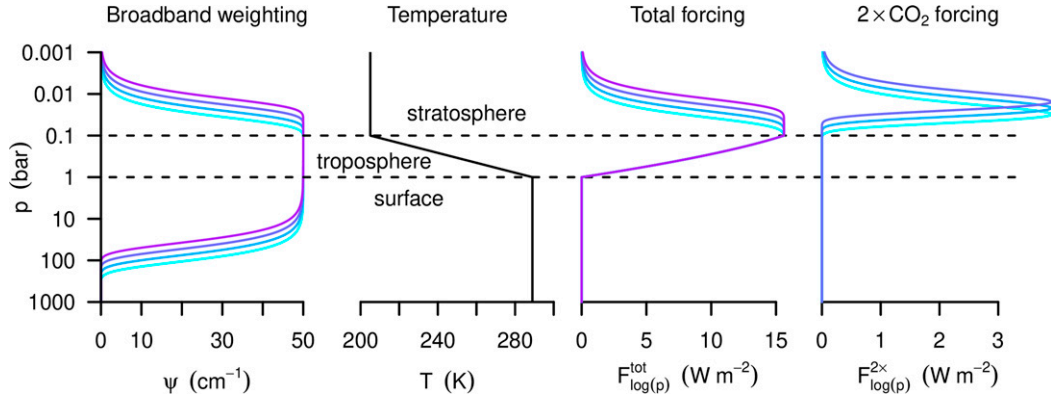
FIG. 15. For 256 ppmv (cyan) to 2048 ppmv (purple) in powers of 2 using the best-fit values for b and κ_0 from section 5b, (from left to right) the broadband weighting function ψ from Eq. (18), the temperature profile in the IsoStrat atmosphere, the total baric (per logarithm of pressure) forcing $F_{\log(p)}^{\text{tot}}$ from Eq. (25), and the baric forcing from a doubling of concentration $F_{\log(p)}^{2\times}(p,q) \equiv F_{\log(p)}^{\text{tot}}(p,2q) - F_{\log(p)}^{\text{tot}}(p,q)$, respectively.

$$F_{\log(p)}^{\text{tot}}(p,q) = \psi(p,q)\pi\left[B(T_{\text{surf}}) - B(T(p))\right] \qquad (25)$$

is what we will refer to as the total baric forcing ["baric" denoting per $\log(p)$ interval, just as "spectral" implies per wavenumber interval]. In particular, $F_{\log(p)}^{\text{tot}}(p,q)d\log(p)$ is the contribution to the total forcing caused by emission to space coming from between $\log(p)$ and $\log(p) + d\log(p)$ instead of from the surface. Note that a $\log(p)$ interval contributes to the forcing only if there is emission to space from that interval [i.e., if $\psi(p, q) > 0$] and if the temperature in that interval differs from the surface [i.e., if $T(p) \neq T_{\text{surf}}$]. The third panel of Fig. 15 plots $F_{\log(p)}^{\text{tot}}(p,q)$ and the fourth panel plots $F_{\log(p)}^{2\times}(p,q) \equiv F_{\log(p)}^{\text{tot}}(p,2q) - F_{\log(p)}^{\text{tot}}(p,q)$. Note that all of the contribution to $F_{\log(p)}^{2\times}$ is in the stratosphere: the total forcing is increased by the introduction of new sets of wavenumbers emitting to space from the stratosphere. Note that the shape of the troposphere temperature profile does not matter for $F^{2\times}$: all that matters is the temperature difference between the train's head and rear, which are in the stratosphere and surface, respectively.

Equations (7), (18), and (20) form a simple model for the radiative forcing of carbon dioxide that can be used to estimate the forcing (for concentrations in the range of 4 to 4096 ppmv) in any atmosphere (in which there are no clouds, aerosols, or other greenhouse gases). The left panel of Fig. 16 shows $F^{2\times}$ calculated from this simple model for various concentrations in the IsoAtmo, IsoStrat, and StdAtmo atmospheres. The IsoAtmo forcing matches the boxcar prediction of 5 W m^{-2} because the head and rear of the wavenumber train are well within regions of the atmosphere with temperatures of 205 and 289 K, respectively. The IsoStrat and StdAtmo forcings start at a lower value of 4 W m^{-2} at 4 ppmv because the head of the train is in the upper troposphere, which is warmer than the tropopause. The StdAtmo forcing peaks when the head of the train is near the cold-point tropopause; since temperature rises with height in the StdAtmo stratosphere, further increases in concentration lead to a

decrease in $F^{2\times}$. For all three cases, however, $F^{2\times}$ remains around 4–5 W m^{-2} over 10 doublings of concentration.[6] The right panel of Fig. 16 plots F_{tot} relative to a concentration of 4 ppmv to illustrate how similarly logarithmic all three cases are.

8. Behavior of the real case

In the preceding sections, we learned that the simple model's broadband weighting function ψ has a magnitude of $2/b$ and it shifts to lower $\log p$ by $\log(2)/2$ for every doubling of q. In other words,

$$\psi(p,q) = \psi\left(\log p + \frac{1}{2}\log q\right) \approx \frac{2}{b}. \qquad (26)$$

We should expect the real ψ, as calculated by a line-by-line model, to approximately exhibit these same properties.

To calculate ψ from a line-by-line model, we need the emission pressures for a dense sampling of wavenumbers. The profile of the absorption coefficient κ is first obtained from the line-by-line model. That κ profile (m^2 mol^{-1}) is then multiplied by the number density of carbon dioxide (with units of mol m^{-3}) and integrated over height to get the τ profile, at which point we can find the pressure where τ equals one. Once we have these emission pressures ($p_{\text{em},i}$ indexed from 1 to 40 001 to cover 467 to 867 cm^{-1} sampled at 0.01 cm^{-1}), we evaluate the integral in Eq. (15) to get the broadband weighting function:

---

[6] It is worth emphasizing how very logarithmic all of these cases are. When F^{tot} is perfectly logarithmic, i.e., $F^{\text{tot}} \sim \log(q)$, then the ratio of the maximum $F^{2\times}$ to the minimum $F^{2\times}$ over these 10 doublings is one: $[\log(4096) - \log(2048)]/[\log(8) - \log(4)] = 1$. This is the case for IsoAtmo. For StdAtmo, the ratio exhibited in Fig. 16 is about $5/4 = 1.25$, which is quite close to one. In contrast, if $F^{\text{tot}} \sim q$, as in the case of very weakly absorbing gas, the ratio over 10 doublings would be $(4096 - 2048)/(8 - 4) = 512$. Or, if $F^{\text{tot}} \sim \sqrt{q}$, the ratio would be $(\sqrt{4096} - \sqrt{2048})/(\sqrt{8} - \sqrt{4}) = \sqrt{512} \approx 23$.
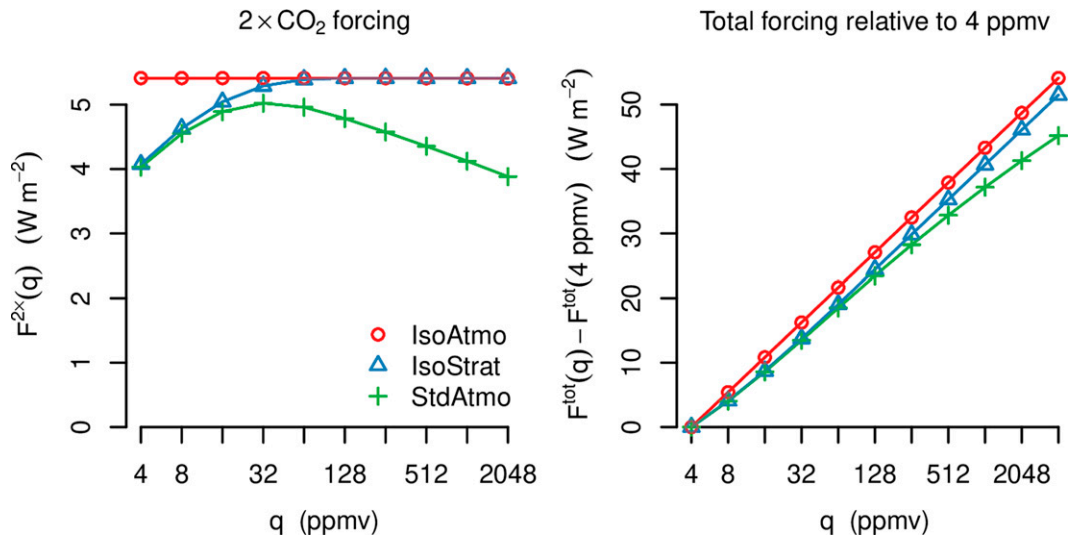
FIG. 16. (left) $F^{2\times}$ calculated from Eqs. (7), (18), and (20) using $\kappa_0 = 8.4 \times 10^{-15}$ m^2 mol^{-1} and $b = 0.04$ cm for the IsoAtmo, IsoStrat, and StdAtmo atmospheres. (right) As in the left panel, but for F^{tot}.

$$\psi(p,q) = (0.01\,\text{cm}^{-1}) \sum_{i=1}^{40\,001} 2 \exp\!\left(-\frac{p^2}{p_{\text{em},i}(q)^2}\right)\frac{p^2}{p_{\text{em},i}(q)^2}. \quad (27)$$

Figure 17 plots this broadband weighting function at CO_2 concentrations ranging from 4 to 4096 ppmv in the StdAtmo atmosphere. Although the shape of this line-by-line ψ has more wiggles[7] than in the simple model's ψ of Fig. 15, we see, as expected, that the line-by-line ψ covers the same-sized swath of $\log(p)$, it has an overall magnitude of about $2/b = 50$ cm^{-1}, and it moves down the $\log(p)$ axis by $\log(2)/2$ for every doubling of concentration [for the 10 doublings shown, ψ shifts a total distance of $10\log(2)/2$].

Consequently, the line-by-line model generates forcings that are similar to those generated by the simple model. The top row of Fig. 18 plots the total baric forcing $F^{\text{tot}}_{\log(p)}$ produced by this line-by-line ψ for each of three atmospheres (IsoAtmo, IsoStrat, and StdAtmo) for CO_2 concentrations ranging from 256 to 2048 ppmv by powers of two. Comparing to the total baric forcing in Fig. 15, we see that the line-by-line model increments the forcing in a way that closely resembles the prediction from the simple model. The bottom row of Fig. 18 plots the TOA forcing as calculated by the line-by-line model for each of the three atmospheres. We see, as expected, that the forcing is still logarithmic in the IsoAtmo atmosphere even without a tropospheric lapse rate. We also see that the

---

[7] At low CO_2 concentrations, the wavenumbers with the lowest absorptivity (near the edges of the 15-μm band) emit to space from deep in the subsurface layer, where extreme collisional broadening has a homogenizing effect on the distribution of κ, causing emission pressures to cluster, which generates the peak in ψ around 100 bar. This high pressure phenomenon has no effect on the forcing since the shape of ψ in the isothermal subsurface has no effect on upwelling fluxes in the atmosphere. The subsurface ψ is plotted only to illustrate the fraction of wavenumbers that are in the surface.

magnitude of the forcings is largely independent of the atmospheric temperature profile (so long as the range of temperatures is the same), and that the magnitude agrees with that predicted by the simple model.

9. Lapse-rate theory is not relevant to carbon dioxide

In contrast to the success of the simple model constructed in sections 3–7, we will see here that the lapse-rate theory is neither *necessary* nor *sufficient* as an explanation for the logarithmic forcing of carbon dioxide. The derivation of the lapse-rate theory is as follows. As discussed in section 5d, τ is proportional to qp^2. Approximating the tropospheric
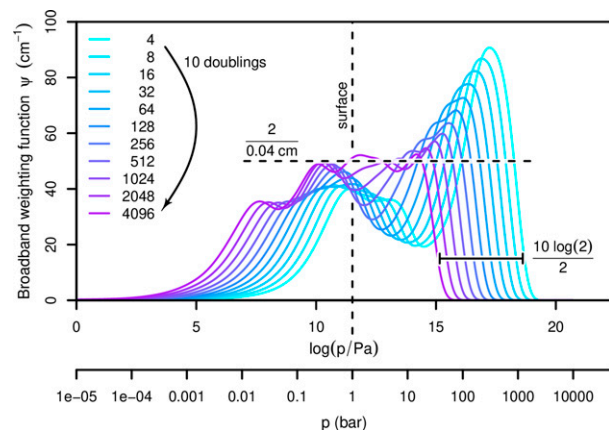

FIG. 17. As calculated from the line-by-line model, the broadband weighting function ψ for the 15-μm CO_2 band in StdAtmo for CO_2 concentrations ranging from 4 to 4096 ppmv by 10 factors of 2. Marked on the plot is the value of $2/b$ diagnosed from Fig. 8. Also indicated is $10\log(2)/2$, which is the distance that ψ is expected to move down the $\log(p)$ axis after 10 doublings of the CO_2 concentration.
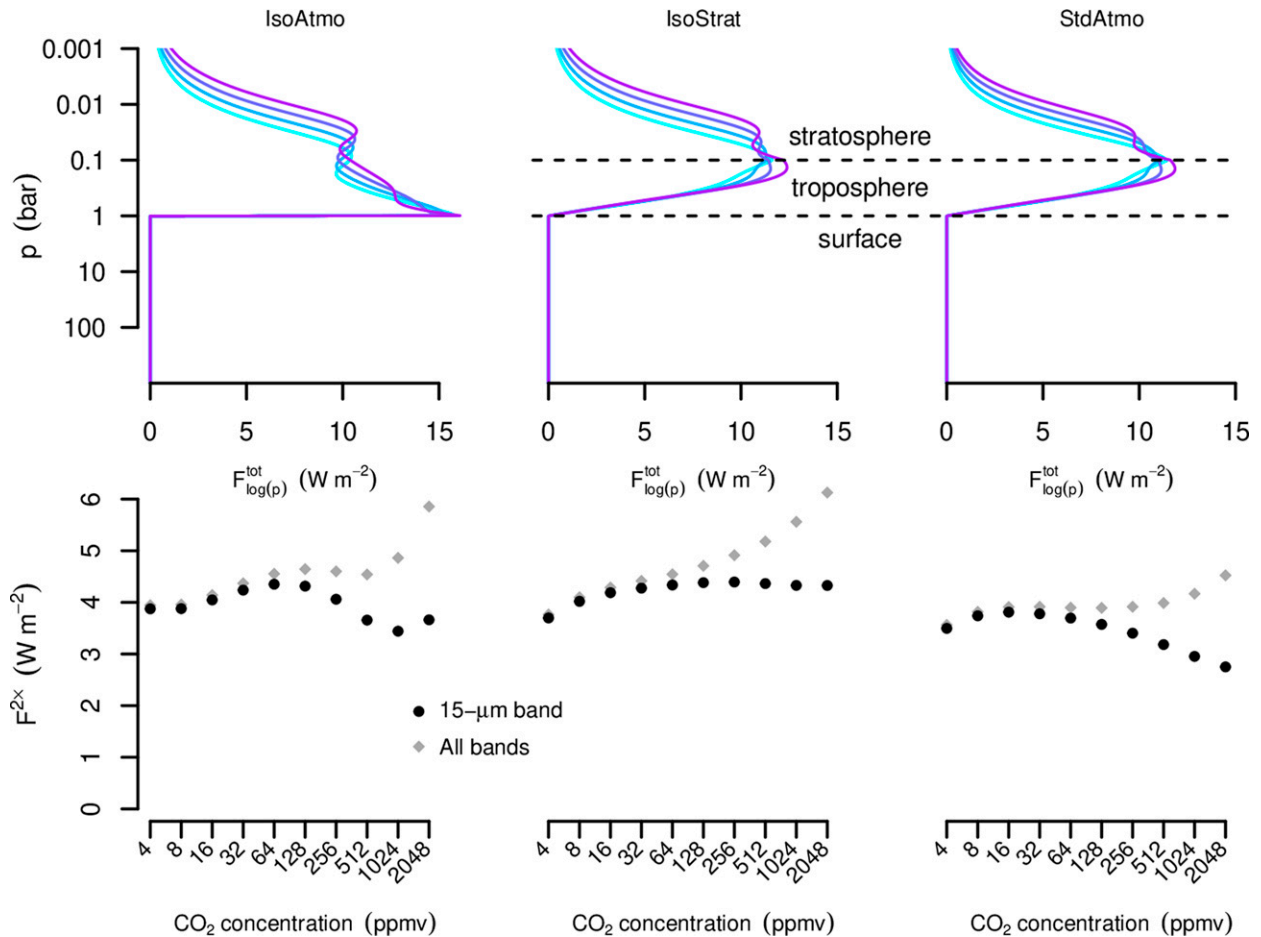
FIG. 18. (top) Plots of the total baric (per logarithm of pressure) forcing $F_{\log(p)}^{\text{tot}}$ calculated with the line-by-line model for CO_2 concentrations ranging from (cyan) 256 ppmv to (purple) 2048 ppmv by factors of 2 for the (left) IsoAtmo, (center) IsoStrat, and (right) StdAtmo atmospheres. The area to the left of each of these curves is equal to F^{tot}. Compare these curves to the plots of $F_{\log(p)}^{\text{tot}}$ in the simple model in Fig. 15. (bottom) Gray diamonds plot $F^{2\times}$ calculated with the line-by-line model and black circles show the contribution to $F^{2\times}$ from the 15-μm band. Compare these data to the plots of $F^{2\times}$ in the simple model in Fig. 16.

temperature profile as $T = T_{\text{surf}} + \Gamma\log(p/p_{\text{surf}})$ for some constant Γ (with units of K), then $p = p_{\text{surf}}\exp[(T - T_{\text{surf}})/\Gamma]$ and $\tau \propto q\exp(2T/\Gamma)$. Solving for the emission temperature T_{em} where $\tau = 1$, we get $T_{\text{em}} \sim -\Gamma\log(q)$. To the extent that the Planck distribution can be approximated as linear in temperature (i.e., $B \sim T_{\text{em}}$), then the spectral flux emitted to space is linear in $-\Gamma\log(q)$, and so the total forcing is linear in $\Gamma\log(q)$.

This derivation did not require a uniform distribution of $\log(\kappa)$, but it does implicitly assume that all of the wavenumbers contributing to the forcing remain in the troposphere as q is varied. Since the wavenumber train of carbon dioxide's 15-μm band does not satisfy this condition, the lapse-rate theory is inapplicable. In fact, we can go a step further and show that the existence of a tropospheric lapse rate—a key component of the lapse-rate theory—is neither necessary nor sufficient for carbon dioxide's logarithmic forcing.

Lapse-rate theory is not *necessary* to explain the logarithmic forcing of carbon dioxide because the logarithmic forcing

can be retained even in the absence of a troposphere. Figure 19a illustrates this using the simple model with IsoAtmo. As shown in the rightmost panel, $F^{2\times}$ (the area under each $F_{\log(p)}^{2\times}$ curve) is the same for each doubling despite the absence of a troposphere.

Lapse-rate theory is not *sufficient* to explain the logarithmic forcing of carbon dioxide because, even in the presence of a realistic troposphere, the logarithmic forcing is eliminated if the stratosphere and surface have the same temperature. Figure 19b illustrates this using the simple model with HotStrat. Although T_{em} is linear in $\log(q)$ for wavenumbers emitting to space from the troposphere, $F^{2\times}$ is zero because the head and rear of the train are at the same temperature.

10. When can lapse-rate theory be applicable?

The lapse-rate theory can work only when the wavenumbers contributing to the forcing keep their emission levels in the troposphere as q is varied. This is most easily achieved if
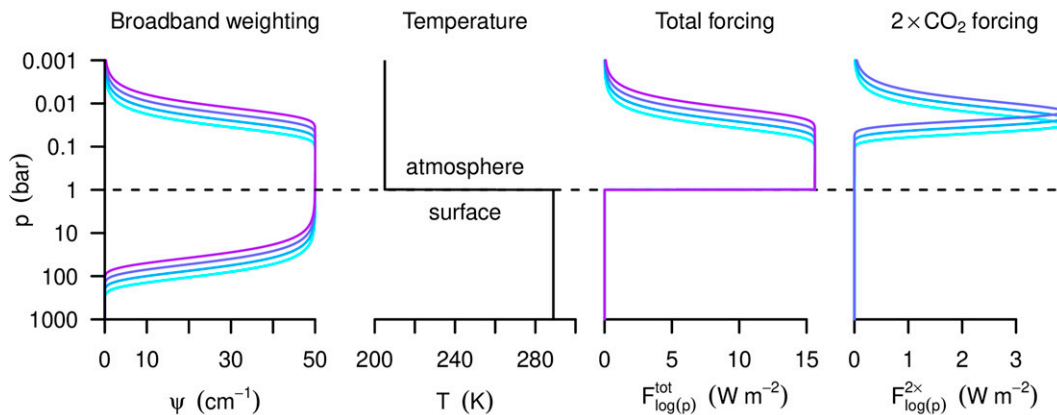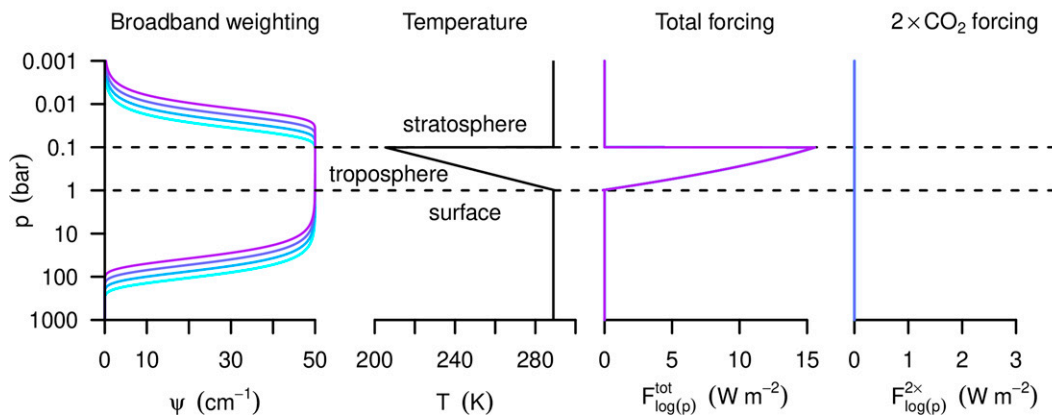
a) IsoAtmo: "Lapse–rate theory" is **not necessary**

b) HotStrat: "Lapse–rate theory" is **not sufficient**

FIG. 19. As in Fig. 15, but for (a) IsoAtmo and (b) HotStrat. These demonstrate that lapse-rate theory is neither necessary nor sufficient to generate the logarithmic forcing from carbon dioxide.

the wavenumbers all have the same emission level (i.e., if they all have the same κ). A hypothetical greenhouse gas that has this property is a best-case scenario for the lapse-rate theory. In this hypothetical case, the spectral weighting function $\phi(\tilde{\nu}, p, q)$ would be independent of $\tilde{\nu}$ within the band, so ψ would simply be the width of the band (in inverse length) times ϕ.

For how many doublings of concentration could this hypothetical band's $\tau = 1$ level remain in the troposphere? The troposphere spans $\log(10)$ in the logarithm of pressure, and, as shown in section 6, each doubling of the gas concentration reduces $\log(p_{em})$ by $\log(2)/2$. Therefore, $\log(p_{em})$ for any given wavenumber can remain in the troposphere for no more than $\log(10)/[\log(2)/2] - 1 \approx 6$ doublings of concentration. This would seem to suggest that the hypothetical gas could produce a logarithmic forcing in Earth's atmosphere—via the mechanism of the lapse-rate theory—over six doublings of concentration.

In fact, however, the logarithmic dependence would not hold for six doublings. The reason why is that the spectral weighting function is not a delta function located at p_{em}, but is

the broad distribution ϕ centered on p_{em}. The spectral weighting function ϕ is so broad that it barely fits inside the troposphere and so nearly always includes significant chunks of either the surface or stratosphere. This is illustrated in Fig. 20.

The left column of Fig. 20 plots ϕ from Eq. (17) for some wavenumber using q equal to $2^{-8}q_0$ (blue), q_0 (red), and $2^8 q_0$ (green), where q_0 is defined to be the concentration that makes $p_{em} = 1$ bar. There are three rows in Fig. 20, each using a different model atmosphere (IsoAtmo, IsoStrat, and Deep-Trop), and the second column plots the temperature profiles of those atmospheres. The third column of Fig. 20 plots the product of ϕ and πB; when integrated over $\log(p)$, this gives the wavenumber's spectral flux to space. The fourth column plots the spectral forcing for this wavenumber from a doubling of q. The circles mark the forcing at every factor of 2 in q. Only in DeepTrop does ϕ fit comfortably inside the troposphere and, therefore, a logarithmic forcing is generated.

Note that Fig. 20 is not specific to carbon dioxide; it applies to any sole well-mixed greenhouse gas with $\kappa \propto p$. If κ is not proportional to p, then matters become even worse for the lapse-rate theory because ϕ is then even broader. While the
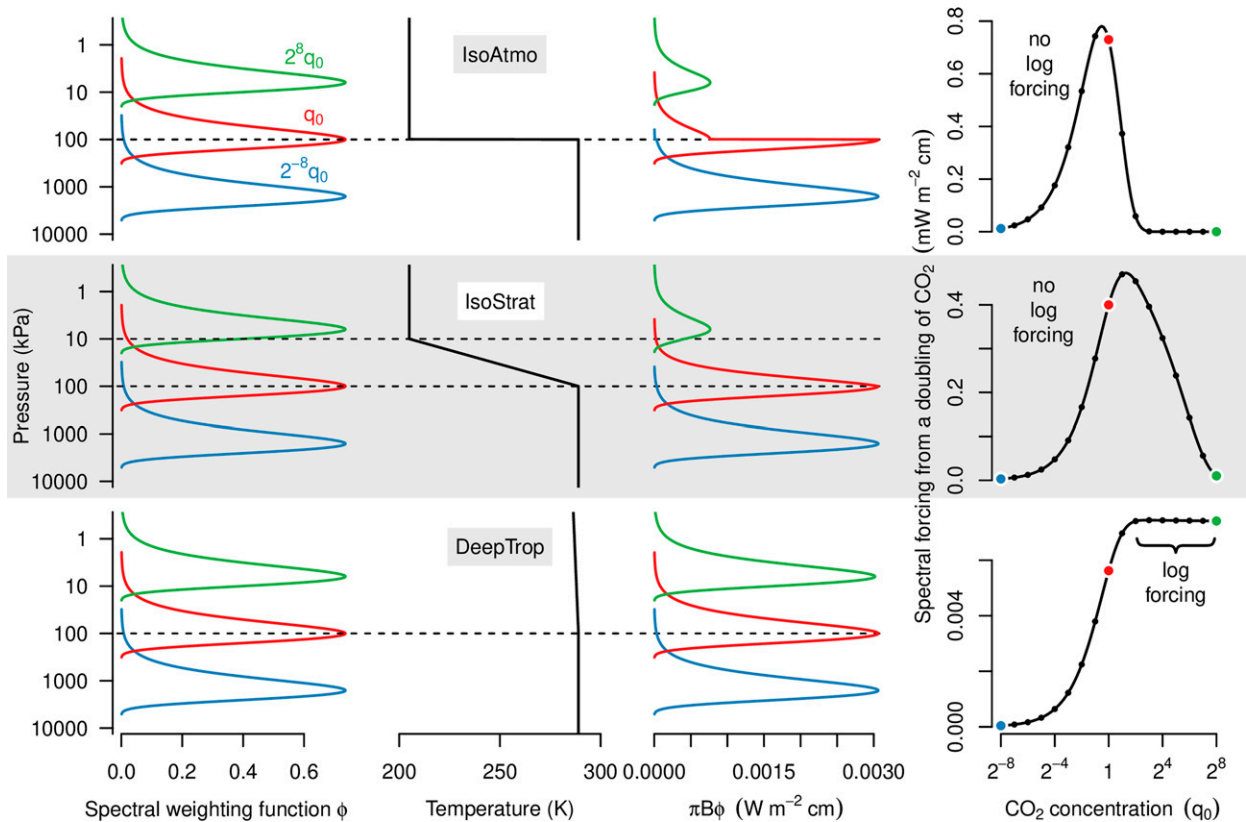
FIG. 20. Illustration of spectral forcing for a single wavenumber for the (top) IsoAtmo, (middle) IsoStrat, and (bottom) DeepTrop atmospheres, with q_0 defined to be the concentration that makes $p_{em} = 1$ bar for the wavenumber. Columns show (from left to right) ϕ from expression (17) for $q = 2^{-8}q_0$ (blue), q_0 (red), and $2^8 q_0$ (green); the temperature profile (for illustration, the surface has been replaced by a 300-K semi-infinite atmosphere); πB times ϕ, i.e., the spectral flux to space; and the spectral forcing, i.e., the difference in spectral flux to space between q and $2q$, as a function of q.

lapse-rate theory does not work for well-mixed greenhouse gases in Earth's atmosphere, it could work in other atmospheres with tropospheres that span a larger $\log(p)$. That would be possible, for example, with a smaller gravitational acceleration or higher specific heat capacity.

11. Summary

Over a wide range of concentrations, the forcing from carbon dioxide is approximately logarithmic in its concentration. It is tempting to attribute this behavior to the troposphere's lapse rate, but this is not the correct explanation. Indeed, the forcing from carbon dioxide is largely independent of the tropospheric temperature profile (see Figs. 16 and 18) and its logarithmic dependence persists even when the atmosphere is isothermal (so long as the surface is warmer; see the IsoAtmo results in Figs. 16 and 18).

Instead, the logarithmic forcing of carbon dioxide can be understood by analogy to a freight train carrying the wavenumbers of the 15-μm band (which dominates the forcing by property 1) from the surface to the stratosphere. The train cars hold same-sized sets of wavenumbers (property 2) grouped by their coefficient of absorptivity; or, more

accurately, the train cars carry same-sized chunks of the emission to space, $\psi d\log(p)$, as defined in Eq. (15). Since the train cars all move together by $d\log(p_{em}) = -d\log(q)/2$ (property 3 combined with $\kappa \propto p$ from pressure broadening), and since the head of the train is in the stratosphere and the rear is on the surface (property 4), and since the radiative emission to space dims the same for all the cars as they rise (property 5), each doubling of CO_2 concentration effectively moves the same-sized chunk of emission to space from the surface to the stratosphere, reducing the total emission to space by the same amount for each doubling. Thus, we arrive at the well-known empirical fact that the total forcing from carbon dioxide scales as the logarithm of its concentration. Using ψ (the broadband weighting function for emission to space) and $F_{\log(p)}^{tot}$ (the total baric forcing, which depicts where in the atmosphere the forcing is generated), we can visualize the underlying mechanism for this logarithmic forcing in both a simple model (Fig. 15) and a line-by-line model (Figs. 17 and 18).

APPENDIX

The Broadband Weighting

To derive the broadband weighting ψ for carbon dioxide, let us make two observations. First, the expression for ϕ in Eq. (17) can be written as

$$\phi = 2e^{-e^{2x}}e^{2x},$$

where $x \equiv \log(p) - \log(p_{em})$. Second, using the expression for p_{em} in Eq. (7), we can deduce that $d\log(p_{em})/d\tilde{\nu} = -b/2$. Using these two facts, we can calculate the broadband weighting function for the 15-μm band of CO_2 (in an atmosphere where well-mixed CO_2 is the only greenhouse gas) as follows:

$$\psi(p,q) = \int_{\tilde{\nu}_1}^{\tilde{\nu}_2} d\tilde{\nu}\,\phi(\tilde{\nu},p,q) \tag{A1}$$

$$= \int_{\log p_{em}(\tilde{\nu}_1,q)}^{\log p_{em}(\tilde{\nu}_2,q)} d\log(p_{em}) \left(\frac{d\log(p_{em})}{d\tilde{\nu}}\right)^{-1} \phi \tag{A2}$$

$$= -\frac{2}{b} \int_{\log p_{em}(\tilde{\nu}_1,q)}^{\log p_{em}(\tilde{\nu}_2,q)} d\log(p_{em})\,\phi \tag{A3}$$

$$= \frac{2}{b} \int_{\log p - \log p_{em}(\tilde{\nu}_1,q)}^{\log p - \log p_{em}(\tilde{\nu}_2,q)} dx\, 2e^{-e^{2x}}e^{2x} \tag{A4}$$

$$= -\frac{2}{b} \int_{\log p - \log p_{em}(\tilde{\nu}_1,q)}^{\log p - \log p_{em}(\tilde{\nu}_2,q)} d\left(e^{-e^{2x}}\right) \tag{A5}$$

$$= \frac{2}{b} \left[e^{-p^2/p_{em}(\tilde{\nu}_1,q)^2} - e^{-p^2/p_{em}(\tilde{\nu}_2,q)^2} \right]. \tag{A6}$$

REFERENCES

Augustsson, T., and V. Ramanathan, 1977: A radiative-convective model study of the CO_2 climate problem. *J. Atmos. Sci.*, **34**, 448–451, https://doi.org/10.1175/1520-0469(1977)034<0448:ARCMSO>2.0.CO;2.

Berner, R. A., 2006: GEOCARBSULF: A combined model for Phanerozoic atmospheric O_2 and CO_2. *Geochim. Cosmochim. Acta*, **70**, 5653–5664, https://doi.org/10.1016/j.gca.2005.11.032.

Cousin, C., R. Le Doucen, C. Boulet, and A. Henry, 1985: Temperature dependence of the absorption in the region beyond the 4.3-μm band head of CO_2. 2: N_2 and O_2 broadening. *Appl. Opt.*, **24**, 3899–3907, https://doi.org/10.1364/AO.24.003899.

Crisp, D., S. B. Fels, and M. D. Schwarzkopf, 1986: Approximate methods for finding CO_2 15-μm band transmission in planetary atmospheres. *J. Geophys. Res.*, **91**, 11851–11866, https://doi.org/10.1029/JD091iD11p11851.

Dudhia, A., 2017: The Reference Forward Model (RFM). *J. Quant. Spectrosc. Radiat. Transfer*, **186**, 243–253, https://doi.org/10.1016/j.jqsrt.2016.06.018.

Edwards, D. K., and W. A. Menard, 1964a: Comparison of models for correlation of total band absorption. *Appl. Opt.*, **3**, 621–625, https://doi.org/10.1364/AO.3.000621.

——, and ——, 1964b: Correlations for absorption by methane and carbon dioxide gases. *Appl. Opt.*, **3**, 847–852, https://doi.org/10.1364/AO.3.000847.

Elsasser, W. M., 1942: *Heat Transfer by Infrared Radiation in the Atmosphere.* Vol. 6. Blue Hill Meteorological Observatory, 107 pp.

Etminan, M., G. Myhre, E. J. Highwood, and K. P. Shine, 2016: Radiative forcing of carbon dioxide, methane, and nitrous oxide: A significant revision of the methane radiative forcing. *Geophys. Res. Lett.*, **43**, 12614–12623, https://doi.org/10.1002/2016GL071930.

Gordon, I. E., and Coauthors, 2017: The HITRAN2016 molecular spectroscopic database. *J. Quant. Spectrosc. Radiat. Transfer*, **203**, 3–69, https://doi.org/10.1016/j.jqsrt.2017.06.038.

Hansen, J., M. Sato, and R. Ruedy, 1997: Radiative forcing and climate response. *J. Geophys. Res.*, **102**, 6831–6864, https://doi.org/10.1029/96JD03436.

Hersbach, H., and Coauthors, 2020: The ERA5 global reanalysis. *Quart. J. Roy. Meteor. Soc.*, **146**, 1999–2049, https://doi.org/10.1002/qj.3803.

Huang, Y., and M. Bani Shahabadi, 2014: Why logarithmic? A note on the dependence of radiative forcing on gas concentration. *J. Geophys. Res. Atmos.*, **119**, 13683–13689, https://doi.org/10.1002/2014JD022466.

Iacono, M. J., J. S. Delamere, E. J. Mlawer, M. W. Shephard, S. A. Clough, and W. D. Collins, 2008: Radiative forcing by long-lived greenhouse gases: Calculations with the AER radiative transfer models. *J. Geophys. Res.*, **113**, D13103, https://doi.org/10.1029/2008JD009944.

Jeevanjee, N., J. T. Seeley, D. Paynter, and S. Fueglistaler, 2021: An analytical model for spatially varying clear-sky CO_2 forcing. *J. Climate*, **34**, 9463–9480, https://doi.org/10.1175/JCLI-D-19-0756.1.

Kiehl, J. T., and V. Ramanathan, 1983: CO_2 radiative parameterization used in climate models: Comparison with narrow band models and with laboratory data. *J. Geophys. Res.*, **88**, 5191–5202, https://doi.org/10.1029/JC088iC09p05191.

Le Doucen, R., C. Cousin, C. Boulet, and A. Henry, 1985: Temperature dependence of the absorption in the region beyond the 4.3-μm band head of CO_2. 1: Pure CO_2 case. *Appl. Opt.*, **24**, 897–906, https://doi.org/10.1364/AO.24.000897.

Mlynczak, M. G., and Coauthors, 2016: The spectroscopic foundation of radiative forcing of climate by carbon dioxide. *Geophys. Res. Lett.*, **43**, 5318–5325, https://doi.org/10.1002/2016GL068837.

Myhre, G., E. J. Highwood, K. P. Shine, and F. Stordal, 1998: New estimates of radiative forcing due to well mixed greenhouse gases. *Geophys. Res. Lett.*, **25**, 2715–2718, https://doi.org/10.1029/98GL01908.

North, G. R., and K. Y. Kim, 2017: *Energy Balance Climate Models.* Wiley, 392 pp.

Pierrehumbert, R. T., 2010: *Principles of Planetary Climate*. Cambridge University Press, 652 pp.

——, 2011: Infrared radiation and planetary temperature. *AIP Conf. Proc.*, Vol. 1401, American Institute of Physics, 232, https://doi.org/10.1063/1.3653855.

Romps, D. M., 2008: The dry-entropy budget of a moist atmosphere. *J. Atmos. Sci.*, **65**, 3779–3799, https://doi.org/10.1175/2008JAS2679.1.

Sloan, T., and A. W. Wolfendale, 2013: Cosmic rays, solar activity and the climate. *Environ. Res. Lett.*, **8**, 045022, https://doi.org/10.1088/1748-9326/8/4/045022.

Stephens, G. L., 1984: The parameterization of radiation for numerical weather prediction and climate models. *Mon. Wea. Rev.*, **112**, 826–867, https://doi.org/10.1175/1520-0493(1984)'112<0826:TPORFN>2.0.CO;2.

Strow, L. L., D. C. Tobin, and S. E. Hannon, 1994: A compilation of first-order line-mixing coefficients for CO_2 Q-branches. *J. Quant. Spectrosc. Radiat. Transfer*, **52**, 281–294, https://doi.org/10.1016/0022-4073(94)90158-9.

Van Vleck, J. H., and V. F. Weisskopf, 1945: On the shape of collision-broadened lines. *Rev. Mod. Phys.*, **17**, 227–236, https://doi.org/10.1103/RevModPhys.17.227.

Wilson, D. J., and J. Gea-Banacloche, 2012: Simple model to estimate the contribution of atmospheric CO_2 to the Earth's greenhouse effect. *Amer. J. Phys.*, **80**, 306–315, https://doi.org/10.1119/1.3681188.

Zhong, W., and J. D. Haigh, 2013: The greenhouse effect and carbon dioxide. *Weather*, **68**, 100–105, https://doi.org/10.1002/wea.2072.